CDF/ANAL/JET/CDFR/1650
4 Feb. 1992
Version 2.0
S. Behrends (Brandeis)
A. F. Garfinkel (Purdue)

X_t Scaling (Updated): Comparison of Jet Production at $\sqrt{s} = 546$ and 1800 GeV

Abstract

This note, an updated edition of CDF-1153, describes the details of the CDF jet scaling analysis, which compares inclusive jet production cross-sections at $\sqrt{s} = 546$ and 1800 GeV. Tests for scaling violation are discussed, and comparisons to theory are made. Results for the cross-section at 546 GeV agree well with UA1 and UA2 when similar definitions for corrected E_t are applied. Statistical techniques for testing the cross-section ratio against the scaling hypothesis indicate that scaling is violated in jet production ($< 5\%$ probability for scaling). Agreement with Next-to-Leading Order QCD calculations for the scaling ratio is good.

1 Introduction

In this note we test the scaling behavior of jet production, which addresses the issue of whether parton-parton hard scattering cross-sections depend in a fundamental way on $\sqrt{s}$ or any other energy-based parameter. The hypothesis of "scaling" predicts that, if we convert to dimensionless quantities for describing jet production, the results will be independent of $\sqrt{s}$. On the other hand, QCD calculations of jet cross-sections depend explicitly on a dimensioned (i.e., non-fractional) energy parameter, Q^2, that characterizes the basic interaction between partons, and whose scale is governed by the outgoing E_t of the interaction. (Alternatively, one can think of this "scale breaking" as arising from the dimensioned parameter Λ_{MS} in the theory.) Physically, this dependence arises from the increased probability of gluon radiation with increasing Q^2, and manifests itself in both the running of the strong coupling constant, $\alpha_s(Q^2)$, and the evolution of the proton structure functions. QCD therefore predicts scaling violation in jet production.

To test the scaling behavior of jet production, we will compare dimensionless inclusive jet cross-sections at two different TEVATRON beam energies, 546 and 1800 GeV. A dimensionless cross-section can be constructed by multiplying the invariant cross-section, $E\frac{d^3\sigma}{dp^3}$, by E_t^4; this is equivalent to multiplying the cross-section we usually measure, $\langle d\sigma/dE_t\rangle_\eta$, by $E_t^3/2\pi$. The dimensionless cross-sections derived from our $\sqrt{s} = 546$ and 1800 GeV jet data-samples will be expressed as functions of the dimensionless energy variable $x_t(\equiv 2E_t/\sqrt{s})$, and the bin-by-bin ratio of these two cross-sections will be used to test the hypothesis of scaling.

Previous tests of jet scaling have been limited either by a small lever-arm in $\sqrt{s}$ [7,8] or by large systematic errors in comparing results from different experiments [10]. CDF is in the advantageous

position of having measured inclusive jet cross-sections at two widely-separated CM energies, 546 and 1800 GeV.

In the next section of this note we describe the data-samples; in the following, the measurement of the cross-section at 546 GeV, with a focus on what we've had to do differently from the 1800 GeV inclusive analysis; Section 4 discusses the measurement of the ratio of 546 and 1800 dimensionless cross-sections, and Section 5 the tests for scaling; in Section 6, we compare to QCD predictions.

2 Data Samples

2.1 Runs and Triggers

The x_t analysis involves two distinct data-sets. The raw 1800 GeV data is identical to that used in the recent 1800 GeV inclusive measurement [9], namely the standard set of merged Jet triggers from the 1988-1989 $4.4pb^{-1}$ run.

The 546 GeV data-sample consists of a set of three runs taken in May 1989: runs 20284, 20296, and 20304. The corrected total luminosity reported from LUMBBC is $7.55nb^{-1}$, where a BBC cross-section of 44mb was assumed. Sebastian White has estimated the ratio of BBC cross-sections, 1800/546, to be (1.30 ± 0.06) [3]. Taking the cross-section at 1800 to be 46.8mb, we obtain a BBC cross-section of 36.0mb at 546 and a total true luminosity of $8.58nb^{-1}$ for the three 546 runs, where this last number has been also scaled down by 7% for the Event_Builder loss. (We note that the full 1800 GeV jet data-set sees only about half of this loss.) We quote the standard 6.8% error on this luminosity, but will refer back to the error on the ratio of BBC cross-sections when we form the ratio of jet cross-sections.

The relevant triggers at 546 were JET-15-CENTRAL (requiring one L2 cluster above 15 GeV in the Central Calorimeter), SUMET-20-CENTRAL (requiring L1 SUMET, calculated in the Central trigger-towers, to be above 20 GeV), and MinBias. We note the non-standard thresholds and η-requirements of the first two triggers, and also mention that data was taken without prescales and thus large deadtime. Two runs at $\sqrt{s} = 1800$ GeV were also taken with these triggers and lack of prescales: runs 20176 and 20185, $0.80nb^{-1}$ total luminosity (NB: the ΣE_t trigger threshold was 30 GeV for these runs). We will refer to these 1800 runs as "1800_*Special*", and they will provide some useful checks of the 546 data (see Section 3).

2.2 Event Selection

Apart from the trigger requirment, the event selection and offline analysis for the two data-sets followed the "standard" path for inclusive jets; we also note that the 546 and 1800 data were processed using the same production executable [19]. Events were required to pass a single-jet trigger, have one or more JETS jets (clustering cone-size = 0.7) in the detector η interval $0.1 \leq$

$|\eta| \leq 0.7$, and have an event z-vertex less than 60 cm from the origin. The vertex-cut efficiency at 546 is estimated to be 91.5%, based on fits to the MBias vertex distributions, as compared to the 94.5% found for the 1800 inclusive analysis: Fig. 1 compares z distributions for inclusive jet events in the 546 and "1800_Special" data, and indicates that the luminous region is indeed somewhat wider for the 546 GeV tune. Background cosmic ray triggers were removed by running HATFLT and CENJET at all $E_t's$. The fraction of events thrown out by HATFLT and CENJET is small at all $E_t's$ for both $\sqrt{s}$ samples. Distributions of JETS ϕ are flat for both inclusive samples. Figure 2 compares JETS η_{det} distributions for jets from the 546 GeV data (E_t>25 GeV) and from the standard 1800 data (E_t>95 GeV), at roughly the same x_t; the distributions are quite similar.

The corrections for energy resolution and degradation for both data-sets follow the standard methodology, documented in a series of CDF notes [17,11,13]. However, as we detail below for the case of the 546 inclusive measurement, the actual corrections themselves incorporate improvements in our understanding and our simulations that have been made since the time of these CDF notes.

3 Inclusive Jet Cross-Section at 546 GeV

The measurement of the inclusive Central jet cross-section at $\sqrt{s}$ = 546 GeV closely follows the analysis performed on the 1988-89 1800 GeV data. In this section we primarily address the few procedural differences that exist between the 546 and 1800 analyses, describe the updated corrections (which will be applied to both data-sets), and present results. Comparison to theoretical predictions will be made in Section 6.

Figure 3 shows the spectrum of jets passing the inclusive cuts for events with $\geq$ 1 jet above 16 GeV, from the 546 dataset. Jets above about 16 GeV constitute single jet inclusive triggers, while below this we see secondary jets in events where a leading jet fired the trigger. This data, above about 25 GeV, will constitute the raw data for our measurement. As an internal check of the 546 data, raw inclusive jet rates vs. E_t (i.e., spectra like Fig. 3 but normalized by luminosity) were constructed for the individual three 546 GeV runs and compared. Agreement between the three runs was quite good, and consistent with the statistical errors of the data-sets.

3.1 JET-15-CENTRAL Trigger Efficiency

We now perform checks on the "non-standard" aspects of the 546 dataset and data-taking procedure – taking data without prescales, and the Central Jet trigger – and estimate the E_t at which the JET-15-CENTRAL trigger becomes efficient.

In Fig. 4a we compare raw inclusive jet rates from the 1800_*Special* runs, the standard 1800 GeV JET-20 data ($4.4pb^{-1}$, prescaled by 300), and also the jets found in the standard 1800 GeV MinBias sample [1]; Fig. 4b takes ratios of these spectra. Above 35 GeV the agreement between the two Jet

triggers is good to 10% or better, indicating that no obvious bias was introduced by taking data without prescales. Unfortunately, the overlap with MinBias is statistically imprecise.

It is important to note that this comparison is also a test of possible time-dependence of Central Calorimeter response (such as might arise from ageing of the scintillator), since the $4.4pb^{-1}$ sample was taken over a 7-8 month period, while the 1800_*Special* runs were from a single day's running late in the run. This issue is of importance because we will be comparing the 546 GeV data (taken the day after the 1800_*Special* runs) to the full $4.4pb^{-1}$ sample of inclusive jets at 1800 GeV.

We see from Fig. 4b that below 35 GeV E_t the JET-20 spectrum becomes inefficient and drops w.r.t. the JET-15-CENTRAL. Naively, we might thus expect the JET-15-CENTRAL trigger to be efficient about 5 GeV lower than the JET-20 trigger, or around 30 GeV. The JET-15-CENTRAL trigger efficiency has been estimated in a more direct fashion by using 546 GeV events that satisfy SUMET-20-CENTRAL. The idea is to look at events which have a Central jet but which triggered independently of that jet, and then to ask how often the jet has an associated L2 cluster above 15 GeV, as a function of JETS E_t. This measures the trigger efficency, barring bugs in the hardware (as a check against this possibility, we note that every JET-15-CENTRAL event has at least one Central L2 cluster with $E_t(L2) \geq 15GeV$).

For SUMET-20-CENTRAL events the sum of Central L2 cluster $E_t's$, $L2SUM$, was formed. Next, for each Central jet in JETS that passed our inclusive jet requirements, we looked for a corresponding L2 cluster, based on requiring the closest match in R, with $R \leq 0.7$. The L2 E_t of the associated cluster (this is 0 if no match is found) was subtracted from $L2SUM$. This result represents "excess" Central L2 cluster energy. If this excess energy was above a certain threshold (roughly 20 GeV), we allowed that Central jet to enter into our measurement of JET-15-CENTRAL efficiency – the idea being that SUMET-20-CENTRAL would have been satisfied by all the excess L2 cluster E_t, had the jet in question not been there.

Figure 5 shows the L2 SUMET distribution (actually calculated at L1) for SUMET-20-CENTRAL events; the sharp edge is at 20 GeV. The JETS-to-L2 association is verified in Fig. 6, where we plot the difference in L2 and JETS centroids ($\delta\eta$: Fig. 6a, $\delta\phi$: Fig. 6b) vs. JETS E_t; the data is well contained within our cut of $R \leq 0.7$. The correlation of L2 and JETS $E_t's$ is shown in Fig. 7. Figure 8 plots the distribution of $L2SUM - E_t^{L2}$ for each JETS cluster passing the inclusive cuts (the events at 0 have only one Central L2 cluster). In Fig. 9 we have restricted ourselves to JETS jets with $L2SUM - E_t^{L2} \geq 22GeV$ and have plotted the fraction of jets with $E_t^{L2} \geq 15GeV$ vs. JETS E_t: this curve represents the efficiency for a single Central JETS cluster to have triggered JET-15-CENTRAL. An efficicency of 90% is obtained at an offline E_t of about 26 GeV.

In Fig. 10 we accept jets within various ranges of $L2SUM - E_t^{L2}$ shown in the key; we see no systematic trend, and conclude that the efficiency determination is free of bias from the SUMET-20-CENTRAL trigger requirement. The data in Fig. 9 were fit to give the single jet efficiency. However, because our inclusive jet events are allowed to have more than one jet in the Central, an overall event-wide efficiency was determined based on the efficiency curve, the number of Central JETS jets found in each event, and their $E_t's$ [4]. The event efficiency for events with a jet at, say,

26 GeV, is typically a few percent higher than the single-jet efficiency at that E_t.

In order to minimize the size of any efficiency correction ($\epsilon \geq 0.9$), and to match with the 1800 GeV data (see Section 4), a cut of $E_t \geq 25.7GeV$ was chosen for the inclusive jet analysis at 546 GeV. A total of 1403 jets pass all requirements. We could cut harder in E_t but only at the expense of reducing our E_t "lever-arm" for the unsmearing process; however, the threshold E_t cut was varied as a check, as we discuss further on.

3.2 Checks of Jet Properties at 546 GeV

If jets of the same E_t were different in 546 GeV events compared to 1800 GeV, it would be inappropriate to apply the standard set of corrections for jet energy and resolution, since these were determined from an MC tuned to 1800 GeV data. We have made several comparisons of 546 and 1800 jet properties, using jets of the same E_t from the 546 and 1800 GeV JET-15-CENTRAL samples. (Although such comparisons should provide the most reasonable measure of the agreement in jet properties, they are limited as a result of different E_t smearing effects for the two samples, which have different E_t spectra.)

Figure 11 shows calorimeter E_t-flow in ϕ w.r.t. the lead jet in JET-15-CENTRAL dijet events [14]; 546 (solid) and 1800 (dash) GeV data are shown. To reduce sensitivity to the different E_t spectra at the two $\sqrt{s}'s$ – which determines the average E_t of the jets in the plot – we have scaled each event's entries by the E_t of the lead jet, and have restricted JETS E_t to the range $27 - 32GeV$. Jet shape is seen to be very similar for the two samples, especially on the scale of the clustering cone (indicated). The difference seen in the away-side jets will be discussed in Section 6.

From Fig. 11, we see there is a difference in the size of underlying event (UE) levels between the two $\sqrt{s}'s$ samples, which we take to be represented by the energy seen around 90^0 in ϕ from the dijet axis. A study by Carol Hawk [14] assessed the level of UE E_t density in JET-15-CENTRAL dijet samples at 1800 and 546 GeV. She finds the 546 GeV sample has $(58 \pm 5)\%$ of the unassociated energy seen in the 1800 GeV sample [2]. The impact of this UE difference will be discussed in the next sub-Section.

In terms of actually quantifying any possible difference in detector response to jets at 546 GeV, Fig. 12 is crucial. Here we plot the estimated loss of jet energy due to calorimeter nonlinearity, as a function of jet E_t. JET-15-CENTRAL data at 546 and 1800 GeV are compared. This estimate is constructed by looping over CTC tracks within a cone of 0.7 around each JETS cluster axis, and forming the jet-by-jet quantity $\Sigma(p_i - CAL(p_i))/E_t^{JETS}$, where CAL is a function representing the average Central calorimeter energy depositied by hadrons with momentum p_i (see Ref. [11] for further discussion). This is a measure of how the fragmentation properties of the jets impact measured jet energy. Jets at the two CM energies show the same loss. We have also compared the average fraction of jet E_t carried by charged particles as a function of jet E_t for the two samples, and good agreement is seen.

3.3 Cross-Section Unsmearing Procedure

Overall, the jet correction/unsmearing process for the 546 data followed the standard prescription [17]. Both energy degradation effects and calorimeter resolution are accounted for simultaneously by the unsmearing process. The result is a "physics curve", which represents the unsmeared true E_t spectrum. This is obtained iteratively, and is defined as the curve which, when smeared by known energy degradation and resolution effects ("Response Functions") and binned in E_t, most closely resembles our measured data. Like the 1987 and 1989 1800 GeV inclusive analyses, the unsmearing procedure corrects back to the E_t of the fragmentated parton; and like the 1989 analysis, we limit the sum to fragmentation products which point within the clustering cone.

3.3.1 Improvements and Modifications to the Procedure

The current analysis of both data-samples benefits from an improved understanding of single-particle calorimeter response and its uncertainty, both at tower-center and in cracks [5,6]. QFL Version 3.10 (and beyond) reflects this new energy-scale and better understanding of Central crack response, and has been used to generate high-statistics samples of simulated jets for the re-determination of parton Response Functions. The path used in the MC production was SIMJET (central dijets) + SETPRT + QFLANA + QTKEFF + JETCLU. (SETPRT fragments the SIMJET partons, and QTKEFF imposes tracking inefficiency on charged particles.) This high-statistics MC sample has enabled us to improve the Response Function parametrizations by allowing both upward- and downward-going exponential tails to be specified (in Ref. [17] only a single Gaussianly-smeared exponential was used). Figure 13 plots JETS E_t distributions for MC jets with $E_t^{true} = 25$ and 290 GeV, together with fitted Response Functions. As described in Ref. [17], we fit such distributions at various values of E_t^{true} between 5-450 GeV, parametrize the E_t dependence of the fit results, and install the parametrizations into the unsmearing package. (The unsmearing package can therefore be thought of as functioning like a quick MC.)

The JETCLU clustering efficiency, expressed as a function of E_t^{true}, is also necessary for the unsmearing package, where it is used as a weight for the Response Functions; it too has come from MC jets, and is shown in Fig. 14. A clustering cone of 0.7 was used, and the underlying event was turned off, in order to avoid over-efficiency at low E_t^{true}.

Slight modifications were made to the Response Functions in order to use them in the 546 GeV unsmearing: because R.F.'s came from tuned 1800 GeV MC, we had to account for the smaller UE E_t density and fluctuations seen at 546 GeV. The former contributes to jet energy scale (i.e. the mean E_t of the Response Functions), the latter to jet E_t resolution. UE E_t adds 1.52 GeV on average to jet E_t at 1800 GeV, and 0.88 GeV to 546 GeV jets (the UE E_t density at 1800 GeV is about 1 GeV per unit area in $\eta - \phi$). We therefore added an E_t-independent shift of -0.64 GeV to the standard relationship of JETS E_t as a function of "True" E_t. Fluctuations in UE E_t are shown in Fig. 15, which compares UE spectra at 546 and 1800 GeV, obtained by summing Central Calorimeter E_t at $90^\circ \pm 10^\circ$ to the thrust axis in ϕ, in JET-15-CENTRAL dijet events

[14]. The area of the slice in $\eta - \phi$ is very close to that of a 0.7 cone. The distribution at both ECM's is nearly exponential, with RMS about equal to mean (1.4 GeV at 1800, 0.8 GeV at 546). (We note that our tuned SETPRT+QFL MC matches the 1800 UE spectrum data quite well.) Because Response Functions represent the JETS E_T distribution at a given true E_t, and since the presence of UE energy only makes JETS E_t larger, the primary impact of UE is on the upward-going tail. Rather than go through the effort of tuning the MC to the 546 UE level, we assessed the UE dependence of R.F.'s in the following way. A sample of MC events were generated with *no* underlying event. Response Functions were determined and compared to the standard (1800 GeV) ones. As expected, the mean E_t's and upward tails were found to be different, most noticibly for $E_t^{true} < 30GeV$; Fig. 16 compares 15 GeV R.F. data and fits for the two samples, where the differences are clearly visible. The parametrization of upward tails used in the 546 GeV unsmearing was taken to lie between the 1800 and no-UE parametrizations (58% was the actual factor used to interpolate between the parametrizations, since this is the "546/1800" ratio of UE RMS's). At 15 GeV, for example, the upward tail of the Response Function (described by an exponential decay constant) was 2.3 GeV from 1800 GeV MC and 1.1 GeV from no-UE MC, and was therefore taken to be 1.8 GeV at 546. Uncertainty in these modifications is a source of systematic error (below).

3.3.2 Checks of the Unsmearing Procedure

A high statistics sample of Central MC jets (1.5 million events), generated with a falling E_t spectrum at $\sqrt{s}$=546 GeV, was used to test the unsmearing procedure. Parameters for the falling spectrum were taken from the results of unsmearing the 546 GeV data (see below). The raw Central JETS spectrum above 25 GeV was determined using the standard cuts listed in Section 2, and was passed as input data to the unsmearing package. The resulting physics curve was then compared to the true E_t (i.e. pre-detector) spectrum. The agreement between the smooth physics curve and the MC data was 10% or better for all E_t.

The MC sample had over eight times the statistics of our 546 GeV sample (for JETS $E_t > 25$ GeV). To test possible pathologies in the unsmearing of smaller statistics samples, the MC data was divided into eight sub-sets and individually unsmeared. The differences in the resulting set of unsmeared curves were consistant with one another within statistical error.

There is also a question of whether the QCD predictions for the 546 inclusive jet spectrum could be approximated by the functional form of our physics curve ($\langle d\sigma/dE_t \rangle_\eta = E_t^{-n}(1 - x_t)^m$), since our implicit assumption is that the true E_t spectrum is of that shape. This form is found to fit theoretical predictions for the spectrum (evaluated at Leading Order) to better than 5% over the E_t interval of interest for the 546 unsmearing (5-100 GeV), for a range of LO and NLO structure functions.

3.4 Results for the 546 Inclusive Cross-Section

Figure 17 compares the uncorrected (measured) and corrected (unsmeared) inclusive jet cross-section at $\sqrt{s}$=546 GeV, averaged over the η_{det} interval 0.1 – 0.7, for JETS $E_t > 25.7$ GeV. The binning used for the data was chosen to match-up with a set of bins, at higher E_t but identical x_t, from the inclusive 1800 cross-section measurement (see Section 4). A set of arrows for each data-point indicate the corrections for E_t and cross-section (defined in [17]). The unsmeared or "physics" curve is given by $\langle d\sigma/dE_t\rangle_\eta = (8.22E+08)E_t^{-4.805}(1-x_t)^{8.349}(nb/GeV)$. The χ^2 of the measured data with the prediction for this data (i.e. the prediction for the "smeared" data) was 7.9 for 8 *d.o.f.*

Results for the unsmeared spectrum were found to be insensitive to the starting E_t used (i.e., whether ϵ-corrected bins at lower E_t were added to the raw spectrum, or whether bins above the nominal 25.7 GeV first bin were removed).

3.5 Systematic Uncertainties on the Cross-Section

The evaluation of systematic error followed the procedure used in the 1800 analysis [13]. Briefly, the procedure is as follows. For each source of systematic error, we modified that source's role in the unsmearing package by $\pm 1\sigma$, and then reperformed the unsmearing. The systematic error on the cross-section from each source is then given by the difference between the resulting unsmeared curve and the standard unsmeared curve, evaluated as a function of E_t.

The following sources of error were identified: (1) Calorimeter uncertainty to pions and electrons/photons (this last is a relatively new addition, relating to uncertainty in QFL's simulation of Central response to low-energy ($P \leq 4GeV$) EM showers, and is described in Ref.[5]); (2) underlying event E_t density and RMS; (3) jet fragmentation tuning in MC (due to modelling of tracking efficiency in jets); (4) jet resolution; (5) JET-15-CENTRAL efficiency correction; and (6) JETCLU clustering efficiency, used by the the unsmearing program.

We discuss sources 1-4 in more detail below. For the trigger efficiency uncertainty, we performed an unsmearing using data with no efficiency correction, and have taken half the resulting deviation from the standard unsmearing as systematic error. To gauge the sensitivity to our MC JETCLU clustering efficiency measurement (Fig. 14), we unsmeared using the efficiency observed in gamma-jet events [20], and found only a negligable (< 1%) deviation from the standard unsmearing.

3.5.1 Energy-Scale Uncertainties and Checks

The effect of sources 1,2 (E_t-effect only),&3 on jet E_t, evaluated using SETPRT MC jets, is shown in Fig. 18. The methodology for deriving these jet E_t-scale uncertainties is described in Ref. [13]. For sources 1&2, the single-particle calorimeter response uncertainties, used as input to this methodology, came from Ref. [5].

The underlying event uncertainty is taken to be $^{+30}_{-50}\%$ of its value. Although the experimental measurement uncertainty is $\pm 30\%$ [15], we raise the error to account for theoretical uncertainty on how much of the UE E_t is actually uncorrelated to jets. HERWIG for example predicts that half of the observable density is of jet origin. Also, as is well known, the Central Calorimeter E_t density observed in MinBias events is about half the level of UE E_t in jet events. Hence our increased *downward* uncertainty of 50%. We note that, for the UE-effect unsmearings, the UE contribution to the upward tail of our Response Functions was also simultaneously scaled by $^{+30}_{-50}\%$, to track with the variation of UE E_t; both E_t-shift and resolution effects will be taken together as "UE uncertainty".

Overall systematic error on jet energy scale, as seen in Fig. 18, totals about $4-5\%$ for jets below 100 GeV. To substantiate this claimed understanding of jet energy scale and errors, we present a few results taken from recent studies of the CDF jet and photon datasets. Brian Winer [12] studied momentum balance in electron+jet events, where the electron is believed to be one leg of an asymmetric conversion pair. The electron E_t interval is $20-60 GeV$, and after applying corrections to jet and UE energies derived from QFL V3.10, E_t balance is maintained at the level of $1-2\%$ for all electron E_t's, as shown in Fig. 19. A similar test at lower $E_t's$ was conducted by Les Nakae and Steve Kuhlmann using gamma-jet events [20]. Figure 20 (21) compares E_t balance in PHOTON-10 (PHOTON-23) gamma-jet events; the quantity plotted is the difference of gamma and jet E_t's parallel to the gamma direction. Also shown are results for Monte Carlo samples of gamma-jet events. These simulated samples used an E_t^γ spectrum like that seen in the data, and included intrinsic "k_t kick" and trigger simulation. Agreement at both energies between data and QFL V3.10 simulation is good, both for the average E_t balance and the shape of the balance distribution.

We have also tested the dependence of the jet energy scale on our tuning of SETPRT jet fragmentation by comparing energy scales from SETPRT and HERWIG. SETPRT was tuned to agree with our fragmentation data, while HERWIG provides QCD-based predictions for fragmentation. The two scales were found to agree to better than 1.5% at all E_t.

3.5.2 Jet Resolution Uncertainties and Checks

For the jet resolution uncertainty, we have separately addressed variations in both the magnitude and shape of the resolution distributions, and have also considered the effect of tuning our Response Functions for 546 UE fluctuations. We have (a) scaled the RMS's of the Response Functions by an overall $\pm 10\%$, (b) used simple Gaussian's for Response Functions, adjusting the standard deviations so as to keep the same RMS's), and (c) performed unsmearings using RF's determined with no UE and with 1800 GeV UE, and have taken the range in results as error. Source (c) is taken to be independent of the UE systematic error described above, since it is intended to account for uncertainty in the interpolation method used to modify the standard R.F.'s for 546 UE level. Because sources (b) and (c) represent bounds on the shape and R.F.-modification effects, we have performed unsmearings and taken one-half of their deviations from the standard unsmearing as

systematic error.

The range of RMS in (a) was arrived at by considering the level of agreement seen above in gamma-jet balance between data and MC (Figures 20&21), and in dijet balance. Fig. 22 compares data and MC predictions for dijet balance at $E_t^{JETS} = 100$ GeV[17,12]. An error of $\pm 10\%$ seems a reasonable value to assign to the MC modelling of the width of jet E_t resolution.

The overall systematic error on the 546 cross-section, including all sources, is about $\pm^{30}_{20}\%$ and is nearly independent of E_t, owing to the small range of E_t subtended by the data. Table 1 presents results for the corrected inclusive cross-section at 546 GeV with a breakdown of systematic error by source.

3.6 Comparison to CERN Measurments

Figure 23 compares our data with results from UA1 and UA2, with systematic errors shown in the key. A definite disagreement between CDF and CERN is apparent. This disagreement is understandable in terms of E_t-scale definition, however. Both CERN experiments corrected jets back to the $E_t(= P_t)$ of the original massless partons from their Monte Carlos, whereas we work back to a coned E_t sum of final state particles from partons. We use final-state sums because we've always believed that converting a masseless parton to a massive jet is black magic – in other words, it is Monte Carlo dependent; and why should we assume the Mind of God lives in the FORTRAN code that Frank Paige wrote for ISAJET? – and we work with *coned* final-state sums in order to compare to $O(\alpha_s^3)$ calculations which have an explicit dependence on clustering cone-size. Also, the charged-particle fragmentation properties of our SETPRT MC jets were tuned only for CTC tracks that point within the clustering cone [11].

But for the sake of making a comparison to CERN's results, we will temporarily adopt a new E_t definition. An unsmearing was performed that corrected back to "total parton E_t", defined as the E_t sum of *all* particles from the parton. Note that, depending on the Monte Carlo program one uses, this quantity may or may not be conserved by the parton fragmentation process – ISAJET for example conserves energy *on average* when it fragments partons, but for any particular parton it is only *approximately* conserved [22] – but this certainly accounts for the energy of fragmentation products lost outside the clustering cone. This unsmearing pass included new jet E_t scale and JETCLU efficiency, determined using this new jet energy definition (apart from their mean $\langle E_t \rangle$'s, Response Functions from the standard analysis were found to be adequate for this test). Figure 24 shows the results of this special unsmearing pass, along with the UA1 and UA2 data. We see excellent agreement between our 546 GeV data and CERN's, well within the quoted systematic errors of the three experiments.

As a final note to the CERN comparison, we mention – with malicious glee, of course – that the published UA1 points are known to be too high in E_t by 5-11% [18]. Translating this error in E_t into the vertical scale would imply that the published cross-section values are roughly 25-70% too high. For this reason, we compare only to UA2 in Figure 25, where our two kinds of corrected data

are shown in the E_t interval of overlap with CERN.

4 The Ratio of 546 and 1800 Jet Cross-Sections

To construct the ratio of dimensionless cross-sections, the two datasets must first have the same binning in x_t. To accomplish this, we actually started with the uncorrected 1800 cross-section ($4.4pb^{-1}$), grouped some of the higher E_t bins together (anticipating the low statistics of our high E_t 546 data), and unsmeared. The resulting set of corrected E_t's for the 1800 bin-edges was scaled by (546/1800) to obtain the corrected bins necessary for the 546 data. The 546 data were then iteratively rebinned and unsmeared until we achieved the desired binning in corrected E_t (to within 0.1% of the desired value). The 1800 bin at $E_t^{meas} = 80.0GeV (E_t^{true} = 88.7GeV)$ specifies the first x_t bin in our scaling comparison, and matches the lowest E_t bin ($E_t^{meas} = 25.7GeV, E_t^{true} = 26.9GeV$) of the 546 sample.

The 1800 cross-section and its errors are given in Table 2, and corrected cross-sections for both the 546 and 1800 GeV datasets are shown together in Fig. 26. The 1800 GeV systematic error shown in the key is the error for that part of the spectrum which overlaps the 546 data in x_t; it nearly constant at about $\pm^{22}_{15}\%$. The sources of systematic error are the same as for the 546 GeV analysis, except for errors due to UE RMS and JET-15-CENTRAL efficiency, which do not apply. The unsmeared or "physics" curve for the 1800 GeV data is given by $\langle d\sigma/dE_t \rangle_\eta = (2.58E9)E_t^{-4.517}(1 - x_t + 0.62x_t^2)^{14.772}(nb/GeV)$. The high statistics of the 1800 GeV dataset has allowed the use of a fourth parameter (x_t^2 term) in the functional form of the physics curve.

The two corrected cross-sections were converted to dimensionless cross-sections vs. x_t. These are shown in Fig. 27. The statistical and systematic errors shown were obtained by scaling the original errors in the same way that the E_t cross-section was scaled; in other words, no additional error is introduced by multiplying the cross-section by $E_t^3/2\pi$. The range of x_t available for comparison is the range subtended by the 546 dataset, 0.102 – 0.268. The bin-by-bin ratio of dimensionless cross-sections, 546/1800, is plotted in Fig. 28. The ratio of physics curves from the unsmearing procedures is shown (solid curve), along with a band of systematic error (dotted curve).

4.1 Systematic Error on the Ratio of Cross-Sections

We now discuss the evaluation of systematic error. Clearly each cross-section has its own set of errors, some of which will partially drop out when we take the ratio. For example, an energy scale uncertainty that is a constant fraction of jet E_t (like an overall calibration uncertainty of the calorimeters) will approximately drop out in the ratio, while an error that is constant in GeV (such as the underlying event energy uncertainty) will contribute to the error on the ratio.

Each individual source of systematic error was varied simultaneously for the two cross-sections, unsmearings were performed, and the ratio of physics curves taken. The deviation of each resulting

ratio from the ratio of standard physics curves defined the systematic error due to that source. The luminosity uncertainty on the ratio, estimated by Sebastian White, contributes an additional 4.6% [3]. The total systematic error is $\pm 17\%$ for the lowest x_t bin, and $\pm 10\%$ for the highest bin. Table 3 presents the ratio data along with a breakdown of the systematic errors. Comparing the three Tables, we see that overall about half of the systematic error on the individual cross-sections cancel in the ratio. While no single source of error is clearly dominant, contributions due to UE and low-P_t electron response uncertainty are generally largest.

5 Scaling Tests

Scaling of jet production predicts that the ratio in Figure 28 should be 1.0. Consistency with this prediction will be investigated using a pair of statistical tests.

5.1 χ^2 Test

To test the scaling hypothesis we evaluated the chi-squared between our data and unity. Using statistical errors alone (which include Poisson errors for the highest x_t bin), we find $\chi^2 = 93.1/11dof$, which would clearly exclude scaling. However, the formation of the chi-squared is complicated by the presence of systematic error, which introduces correlations in the bin-to-bin fluctuations.

Several approaches for including systematic error into the chi-squared determination have been taken. The first is the technique used for the 1987 compositness limit analysis, described in Ref. [21]. With this technique we find $\chi^2 = 19.5/11dof$ (5.3% probability). The second approach is an extension (and improvement) of the first, in which the expression for the off-diagonal elements of the error matrix between bins i and j has been generalized from $\sigma_{ij} = \sigma_i(sys)\sigma_j(sys)$ to $\sigma_{ij} = \Sigma_k \sigma_i(sys_k)\sigma_j(sys_k)$, where k sums over sources of systematic error; this suggestion has come from Mauro Dell'Orso, and reflects the independence of individual sources of error. Using this definition for the σ_{ij}'s, the data has a χ^2 of $17.4/11dof$ (9.6% probability). The correlation is looser in the new approach.

We note that in the above two determinations of chi-squared, systematic uncertainties have been interpretted as "1σ" errors, which in fact they may not be: some sources of systematic error are more akin to absolute bounds, or 2-3σ limits. Our sensitivity to this "1σ" assumption has been tested in the following way. The band of systematic uncertainty shown in Fig. 28 will now be treated as an absolute bound, within which the data can move (coherently) without penalty in χ^2; only statistical fluctuations, however, can take data outside the band. In other words, the error band represents a "box" probability distribution. Evaluating chi-squared in this enviornment is equivalent procedurally to lowering each point by its systematic error (lowered because this direction *lessens* the significance of any scaling violation, and is therefore the conservative direction) and then evaluating chi-squared using statistical errors only. We find $\chi^2 = 32.3/11dof$ (0.1% probability).

We are presently unable to exclude the scaling hypothesis at the 5% confidence level using the χ^2 test.

5.2 Average Ratio Test

Because our values of χ^2 from the above tests are marginal ($< 10\%$ probability), we can perhaps obtain slightly more sensitivity from other tests. A drawback to the χ^2 test is its insensitivity to trends in the data, as in when (for our case) all data-points are consistently above the prediction. Even allowing correlated errors in the χ^2 determination, as we have, the test is still insensitive to trends in the statistical behavior of the datapoints; in other words, if the data in Fig. 28 were moved down by one systematic σ, the majority of points would still be about one statistical σ high. Because the *average value* of the ratio is clearly sensitive to trends, we have pursued this as a test.

For the scaling hypothesis the prediction for the average is 1.0, independent of x_t. To obtain the average value of the ratio from our data, we must make an average that accounts for the different errors of the binned data. In the absense of correlated errors, the correct (minumium error) average is $\Sigma(x_i/\sigma_i^2)/\Sigma(1/\sigma_i^2)$, with an associated error of $\sqrt{1/\Sigma(1/\sigma_i^2)}$. This can be generalized to the case of correlated errors (through maximizing probability of occurence), and one finds the average and error are given by $(\overline{1}\mathbf{V}^{-1}\overline{x})/(\overline{1}\mathbf{V}^{-1}\overline{1})$ and $1/(\overline{1}\mathbf{V}^{-1}\overline{1})^{1/2}$, where $\mathbf{V}$ is the covariance matrix, $\overline{x}$ is the vector of items being averaged, and $\overline{1}$ is a vector with "1" in each place. These expressions reduce to the standard weighted average and error if the covariance matrix is diagonal.

To test the scaling hypothesis given an average value ($< R >$) and error (δ), we construct the significance of deviation from scaling, $(< R > -1.0)/\delta$, and use it to derive the confidence level assuming Gaussian error. As with the χ^2 test, the average ratio was evaluated under various treatments of systematic error. Using statistical errors only, we find the average ratio to be (1.381 ± 0.042); significance and confidence level are 6.7 and $< 10^{-7}\%$. Using the 1987 definition of the covariance matrix, the average is (1.55 ± 0.18), with 3.13 significance and 0.3% CL. Using the updated method for evaluating correlation coeficients, we find (1.52 ± 0.18) with 2.95 significance and 0.4% CL. Lastly, the "box" systematic error envelope definition gives (1.183 ± 0.042), with 4.36 significance and $< 10^{-2}\%$ CL (note that for this case the error is purely statistical).

Based upon the average ratio test, we conclude that our data is inconsistent with the scaling hypothesis at 95% confidence level.

6 Comparison to QCD

A comparison will be made between our data and two orders of QCD predictions. Behavior of the data under changes in the clustering cone-size will also be checked.

6.1 Comparison to L.O. and N.L.O. QCD Predictions

Figure 29 (30) plots our corrected 546 (1800) cross-section data along with a Next-to-Leading-Order calculation of Soper using Morfin-Tung B structure functions and $Q^2 = E_t^2$, and a Leading-Order prediction using an adjusted version of the same structure functions and the same Q^2 choice. The E_t region for the two plots represents the same region in x_t; and for convenience, the cross-section axes span the same number of decades (thus "a factor of 2" looks the same on both plots). Because both theoretical and experimental systematic errors on the cross-sections themselves are relatively large, we will focus on comparing our ratio data to QCD predictions, where both categories of error are reduced. Also, quantatative comparisons will be made to N.L.O. QCD only.

QCD predictions for the ratio vary $5 - 10\%$ over a range of structure function and Q^2 choices. Overall, QCD predicts a roughly constant value of about 1.8 for the ratio. This reflects two effects: (1) the movement to lower x_t ($x_t \leq 0.1$) of the 1800 GeV gluon distribution relative to the 546 gluons (evolution of structure functions), and (2) the higher value of the coupling constant for 546 GeV jets at a given x_t relative to jets of the same x_t at 1800 GeV, which are at higher E_t. In the x_t interval accessible to us, these effects together give a roughly constant ratio, greater than 1.

In Fig. 31 we compare our ratio data to the predictions from the same pair of theoretical calculations used in Figs. 29 and 30. It is also interesting to note that the LO and NLO predictions are so similar to one another, seeming to imply a weak dependence on jet size or cone size (LO jets are single partons, NLO jets are one or two partons); we hope in future to study this issue further using HERWIG MC (i.e. parton-shower model) predictions.

Our data fall somewhat below the ratio predicted by either the LO or NLO theoretical calculations. Using the techniques described Section 5 we have evaluated the χ^2 between our data and a set of predictions. (The average ratio test is not applicable, since the QCD predictions are not constant as a function of x_t.) A set of four structure functions (HMRSE, HMRSB, Tung/Morfin B, and Tung/Morfin S) and a range of Q^2 choices ($4E_t^2$,E_t^2,$E_t^2/4$) were tested, and results are summarized in Table 4. All structure functions tested have $\geq 5\%$ probability using either the 1987 or current definitions of the covariance matrix, for the three choices of Q^2 scale.

6.2 Cone=1.0 Analysis

We must point out the NLO theoretical calculations we compared to above are only approximate, because they lack higher order radiative corrections. Higher order radiation and fragmentation both increase jet size. Also, the limited order of the perturbative part fails to account for the fact that further initial- and final-state radiation produces an effective transverse momentum kick (the so-called "intrinsic k_t") to the Central jets we observe; considered in the framework of an $O(\alpha_s^3)$ calculation, this acts as a further source of smearing on jet E_t. It is empirically seen that this k_t kick is different at 546 and 1800 GeV: This can be seen in the "away-side" of the dijet distributions in Fig. 11, and also in dijet $d\phi$ distributions for the two samples. Jets at the same E_t from the

1800 GeV sample show less "back-to-backness" than the 546 GeV data, or more intrinsic k_t.

The effects of higher order radiation on jet cross-sections should in principle be reduced by using a larger clustering cone. Thus it is interesting to see how our cross-sections and ratio data behave when evaluated with a larger cone-size. The analysis described in Sections 2-4 was redone using JETCLU clustering with a cone-size of 1.0 for both data-samples. This parallel analysis included Monte Carlo determinations of the energy-scale relationship, Response Functions, JETCLU efficiency, and a measurement of the JET-15-CENTRAL efficiency for cone=1.0 JETS jets.

Figure 32 (33) plots raw and corrected 546 (1800) cross-section data for both 0.7 and 1.0 clustering cones. As in Figs. 29&30, the two plots subtend the same x_t interval, and the same number of decades in cross-section. The scaling with cone size of both the raw and corrected data is quite similar at the two $\sqrt{s}$'s. This is reflected in Fig. 34, which shows the cone=1.0 scaling ratio, expressed as the ratio of physics curves from the 1800 and 546 cone=1.0 unsmearings (we did not go so far as to iteratively rebin the cone=1.0 data and form the bin-by-bin ratio) compared with the ratio of curves from the cone=0.7 analysis. Clearly the two results are very similar, just as the LO and NLO predictions were. Again, we hope to investigate this similarity further with HERWIG.

7 Summary

We have measured the inclusive central jet cross-section at $\sqrt{s}$ = 546 GeV. When comparable definitions of corrected jet E_t are adopted, our CDF result agrees well with data from UA1 and UA2. The systematic error on our cross-section is approximately 30%. The ratio of dimensionless cross-sections, "546/1800", was constructed with approximately 15% systematic error, and was tested against the scaling hypothesis. We conclude that the hypothesis of scaling is rejected at the 95% confidence level. Comparisons were made to $O(\alpha_s^3)$ QCD predictions, and good agreement is seen for a range of structure functions and choices of Q^2 scale. We also documented or referenced a number of tests of the jet data-samples and jet corrections that lend credence to our jet cross-section results and for the ratio of dimensionless cross-sections.

References

[1] The MBias jet analysis was performed by Steve Kuhlmann.

[2] We have also compared the central ΣE_t distribution in MinBias events at 546 and 1800 GeV. We find the the ratio of average ΣE_t's, 546/1800, to be (0.76 ± 0.03). NB: The 546 MinBias data has a higher beam-gas background than the 1800 data, because of the low instantaneous luminosity of the 546 runs. To reduce this background for the MinBias central ΣE_t comparison, we required the event z-vertex to be $\leq 35cm$. The average central ΣE_t was stable for harder cuts on z.

[3] CDF-1202: "CDF Luminosity Calibration".

[4] For events with a single Central jet, the weight was given by $1-(1-\epsilon)$; dijets were weighted by $1-(1-\epsilon_1)(1-\epsilon_2)$, where $\epsilon_i = \epsilon(E_t(i))$ for the *ith* jet; and so on, in the fashion "one minus the inefficiency".

[5] See CDF-1344: "Update on Central Calorimeter Response to Pions and Tuning of QFL" for calorimeter response to MinBias pions, and QFL low-P electron study; see CDF-1286: "Central Calorimeter Pion Response in Light of 1990 Test Beam Data" for calorimeter response to Test Beam pions.

[6] CDF-1361: "Central Calorimeter Crack Response: 1990 Testbeam".

[7] G. Arnison et al (UA1 Collaboration), "Measurement of the Inclusive Jet Cross-Section at the CERN $\bar{p}p$ Collider", Physics Letters B172, 461 (1986).

[8] J. A. Appel et al (UA2 Collaboration), "Measurement of the $\sqrt{s}$ Dependence of Jet Production at the CERN $\bar{p}p$ Collider", Physics Letters B160, 349 (1985).

[9] See Tim Hessing's thesis, a.k.a. CDF-1316: "A Search for Quark Compositeness with the CDF Detector at the Fermilab Collider".

[10] F. Abe et al (CDF Collaboration) "Measurement of the Inclusive jet Cross Section in $\bar{p}p$ Collisions at $\sqrt{s}$= 1.8 TeV", Physical Review Letters 62, 613 (1989).

[11] CDF-1131: "Monte Carlo Fragmentation Tuning for Jet Energy and Resolution Analysis".

[12] CDF-1347: "A Brief Note Comparing Jet Data to QFL"

[13] CDF-1247: "Systematic Uncertainties Associated with the Jet Cross-Section".

[14] CDF-1471: "The Underlying Event in Dijets".

[15] CDF-685: "Underlying Event Energy in Clusters".

[16] A technical point: these unsmearing passes used the prediction for the smeared cross-section from the standard unsmearing as their input cross-section file. This was done in order to decouple statistical effects (i.e. the statistical scatter and imprecision of the measured inclusive spectrum) from the determination of systematic uncertainty on the cross-section. Bin-by-bin statistical errors for this input file were assigned to be 20% of the statistical error of the corresponding bins in the actual data; in other words the file used in systematic-error determination carried 25 times the statistical weight of the actual data.

[17] CDF-1132: "Inclusive Jet E_t Spectrum: Energy Corrections and Resolution Unsmearing".

[18] See UA1 Technical Note UA1-TN-86-77 by Randy Sobie (copies available from SOB).

[19] CDF-1380, "Compressed Jet Data Sample from the 1988-1989 Run: QCD Special Project".

[20] CDF-1431: "Jet Studies in the Photon Sample: Volume I".

[21] CDF-747, "Statistics Issues for the Inclusive Jet E_t Paper".

[22] See Steve Kuhlmann's internal Jet Group note, "Using ISAJET to Determine Jet Energy Correction", 30-Nov-1987. I think this was distributed with the 1987 Jet Paper documentation.

Table 1: Inclusive Central Jet Cross-Section at 546 GeV ($\langle d\sigma/dE_t\rangle_\eta$) vs. E_t. Statistical errors are shown, and ± systematic uncertainties are given as percentage effects. Luminosity uncertainty is a constant ±6.8%.

E_t (GeV)	$\langle d\sigma/dE_t\rangle_\eta$ (nb/GeV)	Stat. Err.	Pion (%)	Elec. (%)	UE (%)	Frag. (%)	Tails (%)	Res'n (%)	ϵ_{L2} (%)	RF_{UE}^{546} (%)	Total Sys(%)
27.7	42.28	±2.34	10.3	20.0	17.3	10.5	3.1	9.5		6.0	33.1
			-10.5	-2.5	-13.7	-9.2		-9.1	-4.2	-8.3	-24.6
29.4	25.99	±1.76	10.8	19.4	16.0	10.6	2.7	8.9		5.3	31.9
			-10.5	-2.6	-12.8	-9.3		-8.6	-3.3	-7.5	-23.6
31.0	20.80	±1.52	11.2	18.8	14.8	10.7	2.4	8.3		4.8	30.9
			-10.5	-2.6	-12.0	-9.4		-8.1	-2.6	-6.7	-22.7
32.7	15.74	±1.29	11.7	18.3	13.7	10.8	2.1	7.8		4.3	30.1
			-10.6	-2.7	-11.3	-9.5		-7.6	-1.9	-6.0	-2[illegible]
34.3	10.63	±1.04	12.1	17.8	12.8	10.9	1.8	7.4		3.8	[illegible]
			-10.6	-2.7	-10.7	-9.6		-7.2	-1.2	-5.4	-21.3
36.0	7.198	±0.842	12.5	17.4	11.9	11.0	1.6	7.0		3.4	28.8
			-10.6	-2.8	-10.1	-9.7		-6.9	-0.7	-4.9	-20.8
38.3	5.853	±0.530	13.1	16.9	10.9	11.1	1.3	6.5		3.0	28.2
			-10.7	-2.8	-9.3	-9.8		-6.5	-0.1	-4.1	-20.3
41.6	3.556	±0.405	13.8	16.2	9.6	11.3	1.0	6.0		2.4	27.6
			-10.8	-2.9	-8.5	-10.0		-6.0		-3.3	-19.7
47.2	1.726	±0.165	15.0	15.4	8.1	11.6	0.6	5.3		1.8	27.3
			-10.9	-3.0	-7.3	-10.3		-5.4		-2.3	-19.2
57.6	0.3802	±0.07059	17.2	14.5	6.7	12.2	0.4	4.9		1.3	27.8
			-11.4	-3.3	-6.3	-10.8		-5.1		-1.6	-19.3
72.4	0.06167	+0.02810	19.9	14.3	7.1	12.9	0.9	5.7		2.0	30.1
		-0.01987	-12.3	-3.6	-6.6	-11.4		-5.9		-2.4	-20.7

Table 2: Inclusive Central Jet Cross-Section at 1800 GeV ($\langle d\sigma/dE_t\rangle_\eta$) vs. E_t, for the x_t interval $0.101 - 0.265$. Statistical errors are shown, and $\pm$ systematic uncertainties are given as percentage effects. Luminosity uncertainty is a constant $\pm 6.8\%$.

E_t (GeV)	$\langle d\sigma/dE_t\rangle_\eta$ (nb/GeV)	Stat. Error	Pion (%)	Elec. (%)	UE (%)	Frag. (%)	Tails (%)	Res'n (%)	Total Sys(%)
91.2	0.8467	$\pm$0.0329	14.5	9.3	6.9	9.1	0.3	2.7	21.9
			-8.9	-2.6	-2.4	-8.3		-2.8	-14.7
96.7	0.5906	$\pm$0.0274	14.9	9.1	6.4	9.1	0.2	2.6	21.9
			-9.0	-2.7	-2.1	-8.2		-2.7	-14.6
102.1	0.4373	$\pm$0.0236	15.2	9.0	6.0	9.0	0.1	2.5	22.0
			-9.1	-2.7	-1.8	-8.2		-2.6	-14.6
107.5	0.3273	$\pm$0.0204	15.6	8.9	5.7	9.0	0.1	2.4	22.1
			-9.2	-2.8	-1.6	-8.2		-2.5	-14.6
113.0	0.22231	$\pm$0.00316	15.9	8.8	5.4	8.9		2.4	22.2
			-9.3	-2.8	-1.4	-8.1		-2.4	-14.6
118.4	0.16773	$\pm$0.00274	16.3	8.7	5.1	8.9		2.3	22.3
			-9.4	-2.9	-1.3	-8.1		-2.4	-14.7
126.1	0.10854	$\pm$0.00157	16.8	8.6	4.8	8.8		2.3	22.5
			-9.5	-2.9	-1.1	-8.0		-2.4	-14.7
136.9	0.06341	$\pm$0.00120	17.5	8.6	4.4	8.6		2.3	22.9
			-9.7	-3.0	-0.9	-7.9		-2.3	-14.8
155.2	0.028355	$\pm$0.000477	18.6	8.5	4.0	8.4		2.3	23.6
			-10.1	-3.2	-0.8	-7.7		-2.4	-14.9
189.5	0.006773	$\pm$0.000216	20.5	8.7	3.6	7.8		2.5	25.0
			-10.7	-3.5	-0.8	-7.2		-2.7	-15.3
238.2	0.0011220	$\pm$0.0000637	22.9	9.1	3.5	7.0		3.0	26.9
			-11.6	-3.8	-1.2	-6.5		-3.2	-15.8

Table 3: The ratio of dimensionless jet cross-sections vs. x_t. Statistical errors are shown, and $\pm$ systematic uncertainties are given as percentage effects. Luminosity uncertainty is a constant $\pm 4.6\%$.

x_t	Ratio	Stat. Error	Pion (%)	Elec. (%)	UE (%)	Frag. (%)	Tails (%)	Res'n (%)	ϵ_{L2} (%)	RF_{UE}^{546} (%)	Total Sys(%)
0.101	1.400	$\pm$0.095	1.8	9.8	9.8	1.2	2.9	6.7		6.0	17.5
			-3.7	-0.1	-11.6	-1.0		-6.5	-4.2	-8.3	-17.3
0.107	1.234	$\pm$0.101	1.7	9.4	9.0	1.4	2.5	6.2		5.3	16.4
			-3.6	-0.1	-11.0	-1.2		-6.1	-3.3	-7.5	-16.1
0.113	1.335	$\pm$0.121	1.6	9.0	8.3	1.5	2.3	5.7		4.8	15.4
			-3.5	-0.1	-10.4	-1.3		-5.6	-2.6	-6.7	-15.0
0.119	1.350	$\pm$0.139	1.5	8.6	7.6	1.7	2.0	5.3		4.3	14.5
			-3.4	-0.1	-9.9	-1.4		-5.3	-1.9	-6.0	-14.1
0.126	1.342	$\pm$0.133	1.4	8.3	7.1	1.8	1.8	4.9		3.8	13.7
			-3.3	-0.1	-9.4	-1.6		-4.9	-1.2	-5.4	-13.3
0.132	1.205	$\pm$0.142	1.4	8.0	6.5	2.0	1.6	4.6		3.4	13.0
			-3.3	-0.1	-8.9	-1.7		-4.6	-0.7	-4.9	-12.6
0.140	1.515	$\pm$0.139	1.3	7.6	5.8	2.2	1.4	4.2		3.0	12.1
			-3.2	-0.1	-8.3	-2.0		-4.2	-0.1	-4.1	-11.8
0.152	1.575	$\pm$0.182	1.2	7.1	5.0	2.5	1.1	3.6		2.4	11.2
			-3.1	-0.1	-7.6	-2.3		-3.7		-3.3	-10.9
0.172	1.717	$\pm$0.166	1.0	6.3	4.0	3.0	0.9	3.0		1.8	10.1
			-3.0	-0.1	-6.6	-2.8		-3.1		-2.3	-9.8
0.211	1.580	$\pm$0.298	0.7	5.3	3.0	4.0	0.8	2.4		1.3	9.2
			-2.8	-0.2	-5.5	-3.8		-2.5		-1.6	-9.1
0.265	1.542	+0.703	0.7	4.8	3.5	5.6	1.6	2.6		2.0	10.1
		-0.497	-2.5	-0.2	-5.4	-5.2		-2.8		-2.4	-10.0

Table 4: Results for χ^2 (probability) evaluated between ratio data and NLO QCD predictions. Four structure functions and three Q^2 choices were tested. Results using four definitions of the covariance matrix for the data, $\mathbf{V}$, are shown. Each value of χ^2 is for 11 d.o.f.

Struc. Fun.	Q^2	Stat'l V	1987 V	Improved V	Box V
HMRSB	$E_t^2/4$	179.0(-)	14.2(22%)	14.0(24%)	75.4(-)
	E_t^2	149.4(-)	12.8(31%)	12.6(32%)	57.2(-)
	$4E_t^2$	110.6(-)	11.1(44%)	10.8(46%)	35.4(-)
HMRSE	$E_t^2/4$	94.4(-)	10.7(47%)	10.5(49%)	27.3(0.4%)
	E_t^2	78.6(-)	9.5(57%)	9.3(59%)	19.8(4.7%)
	$4E_t^2$	61.8(-)	8.8(64%)	8.5(67%)	13.3(28%)
MTB	$E_t^2/4$				
	E_t^2	148.8(-)	13.0(29%)	12.8(31%)	56.8(-)
	$4E_t^2$				
MTS	$E_t^2/4$	204.2(-)	15.9(15%)	15.6(16%)	91.9(-)
	E_t^2	166.8(-)	15.2(17%)	14.7(20%)	68.2(-)
	$4E_t^2$	133.3(-)	12.5(33%)	12.1(36%)	48.0(-)

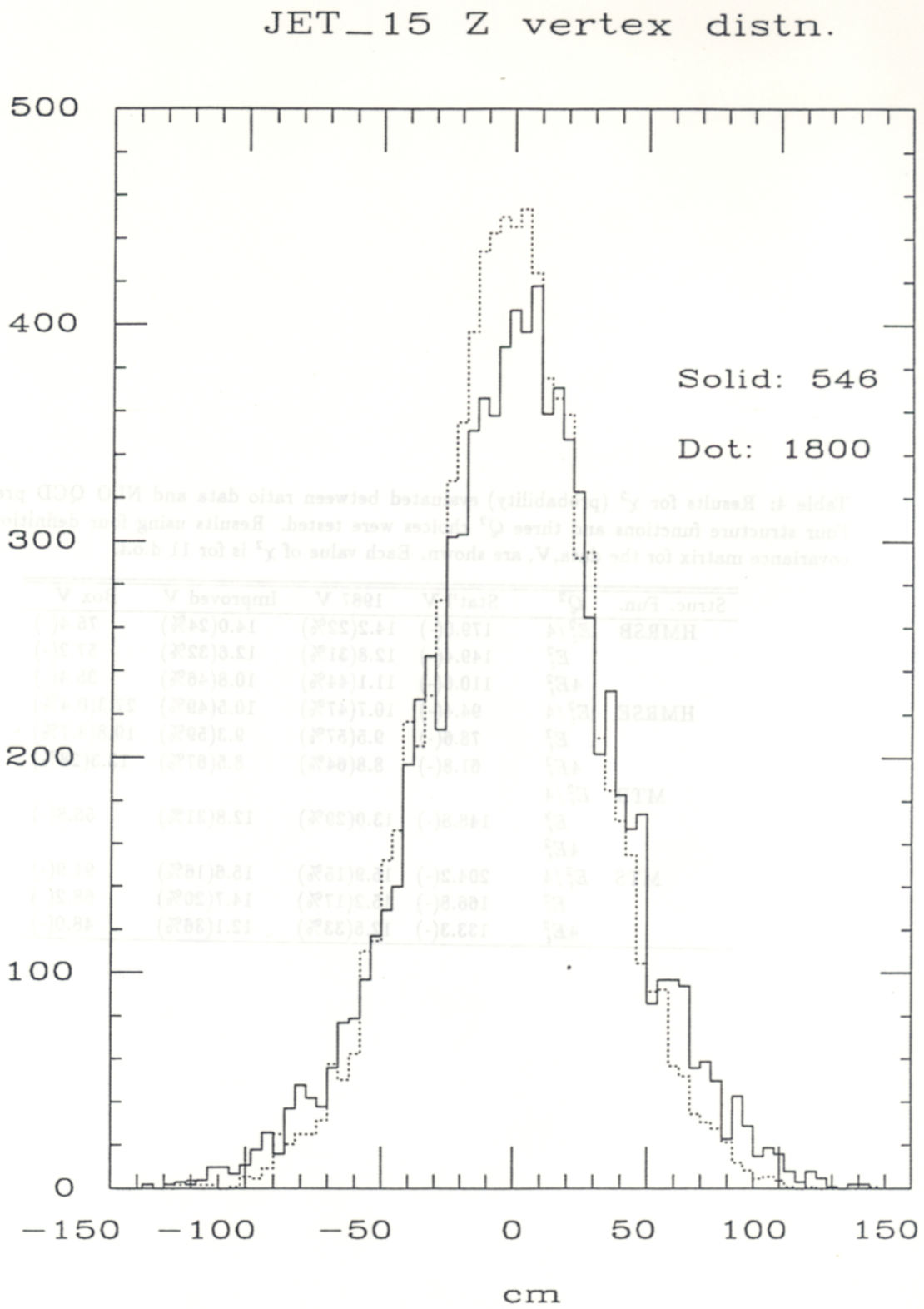
JET_15 Z vertex distn.
500
400
300
200
100
0
−150
−100
−50
0
50
100
150
cm
Solid: 546
Dot: 1800

FIGURE 1

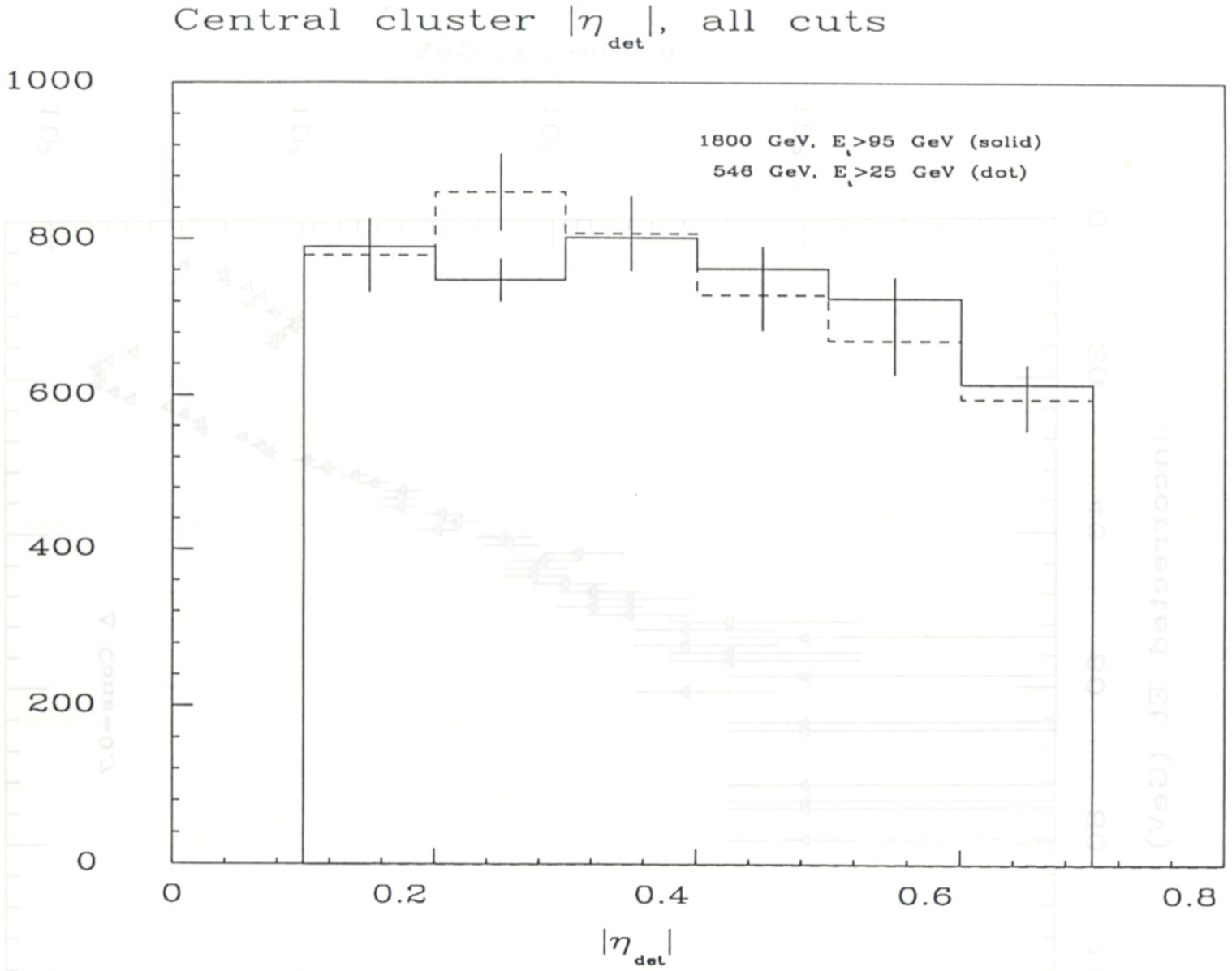
Central cluster $|\eta_{det}|$, all cuts
1800 GeV, E_t>95 GeV (solid)
546 GeV, E_t>25 GeV (dot)
1000
800
600
400
200
0
0
0.2
0.4
0.6
0.8
$|\eta_{det}|$

FIGURE 2

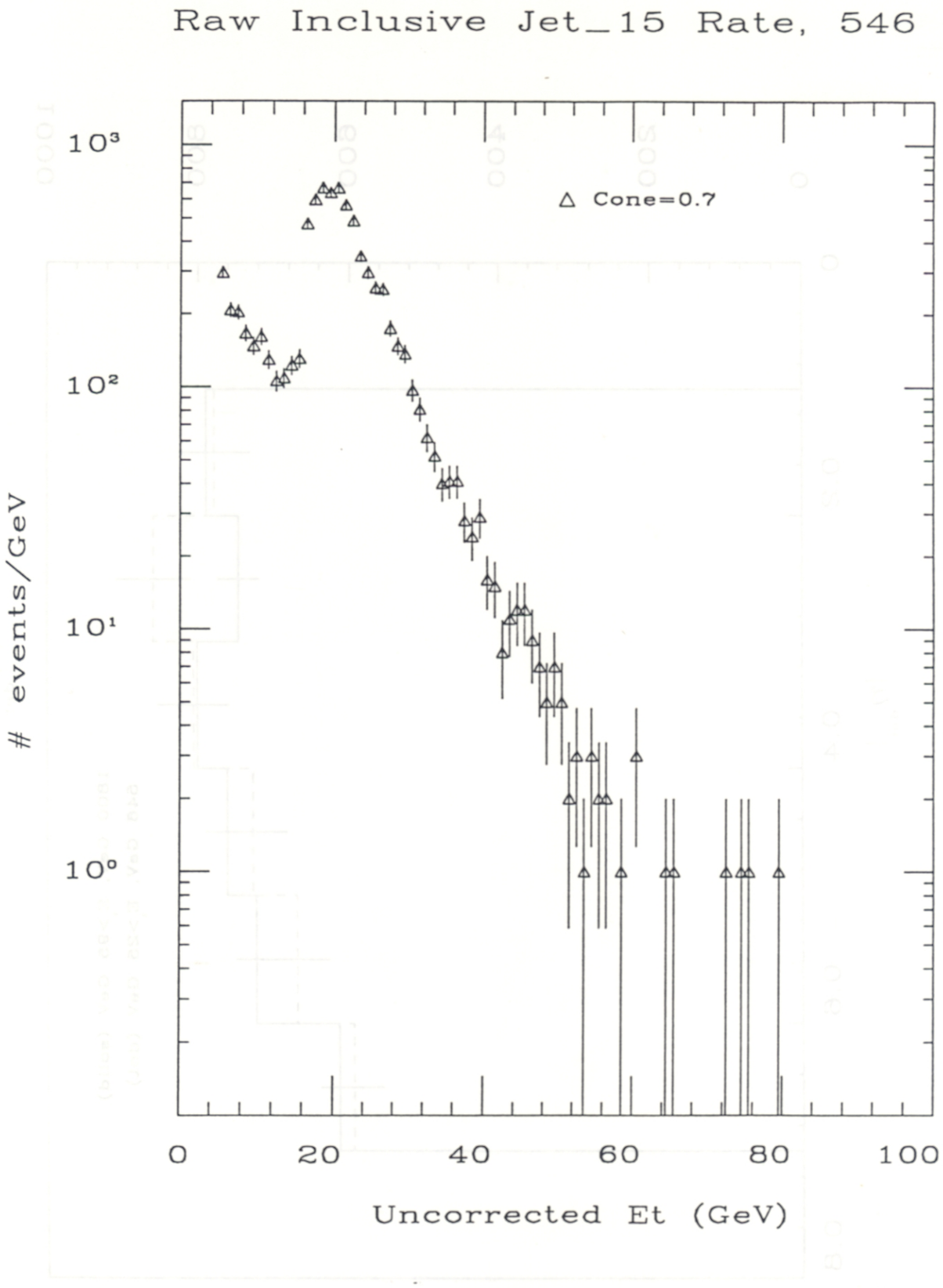
Raw Inclusive Jet_15 Rate, 546 GeV
Cone=0.7
# events/GeV
Uncorrected Et (GeV)
10³
10²
10¹
10°
0
20
40
60
80
100

FIGURE 3

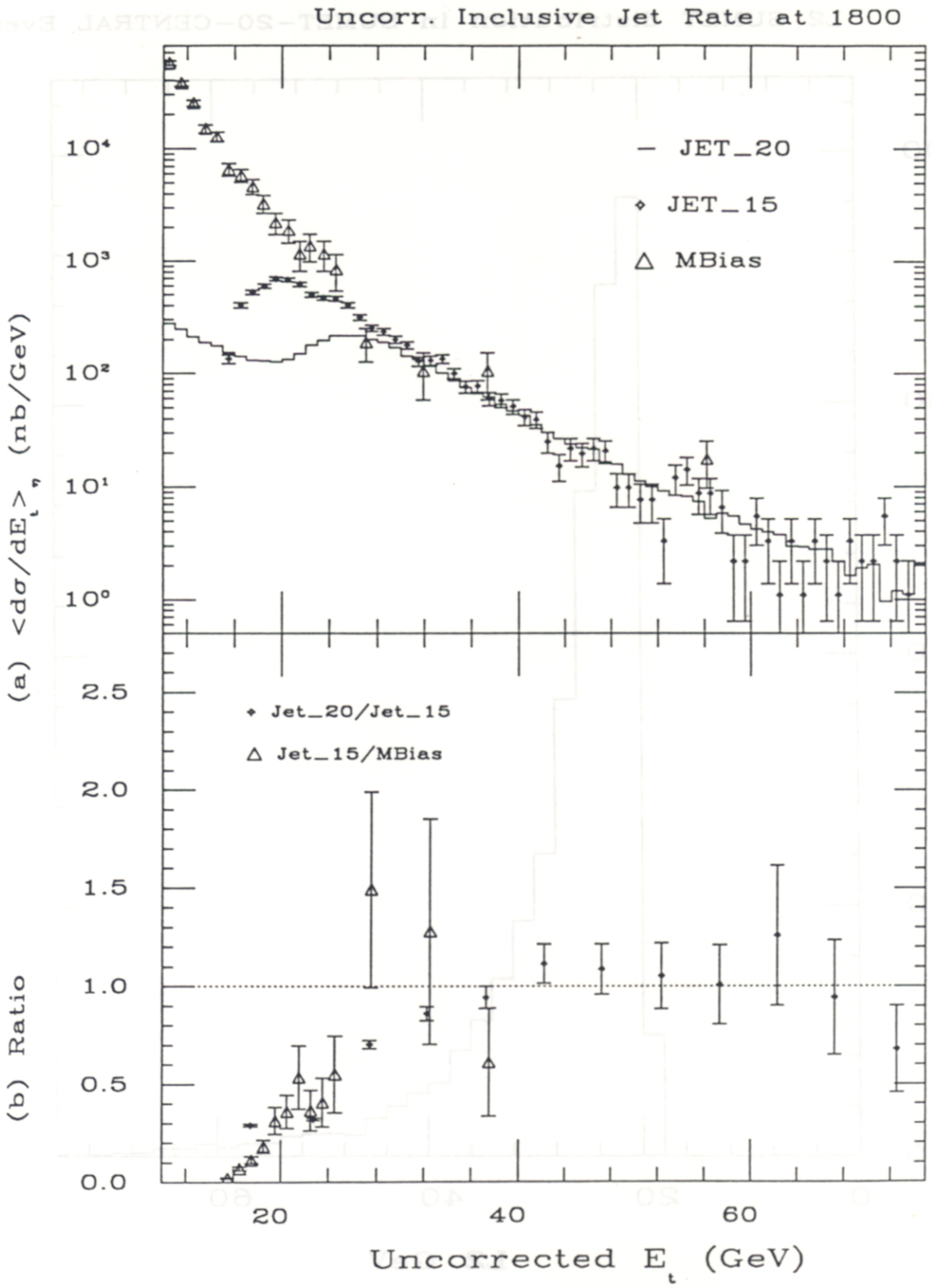
Uncorr. Inclusive Jet Rate at 1800
JET_20
JET_15
MBias
(a) <dσ/dE_t>_η (nb/GeV)
Jet_20/Jet_15
Jet_15/MBias
(b) Ratio
Uncorrected E_t (GeV)

FIGURE 4

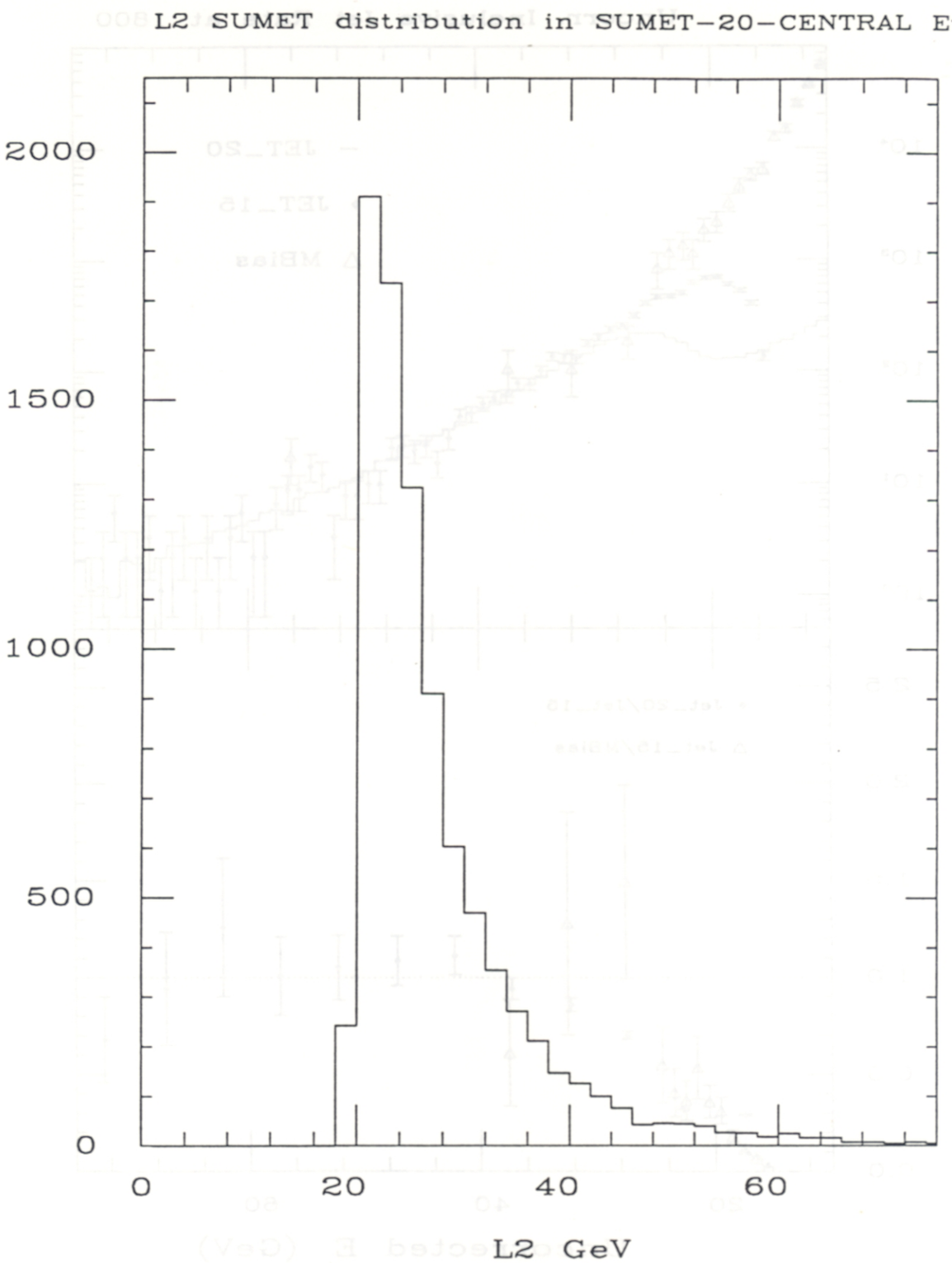
L2 SUMET distribution in SUMET-20-CENTRAL Events
2000
1500
1000
500
0
0
20
40
60
L2 GeV

FIGURE 5

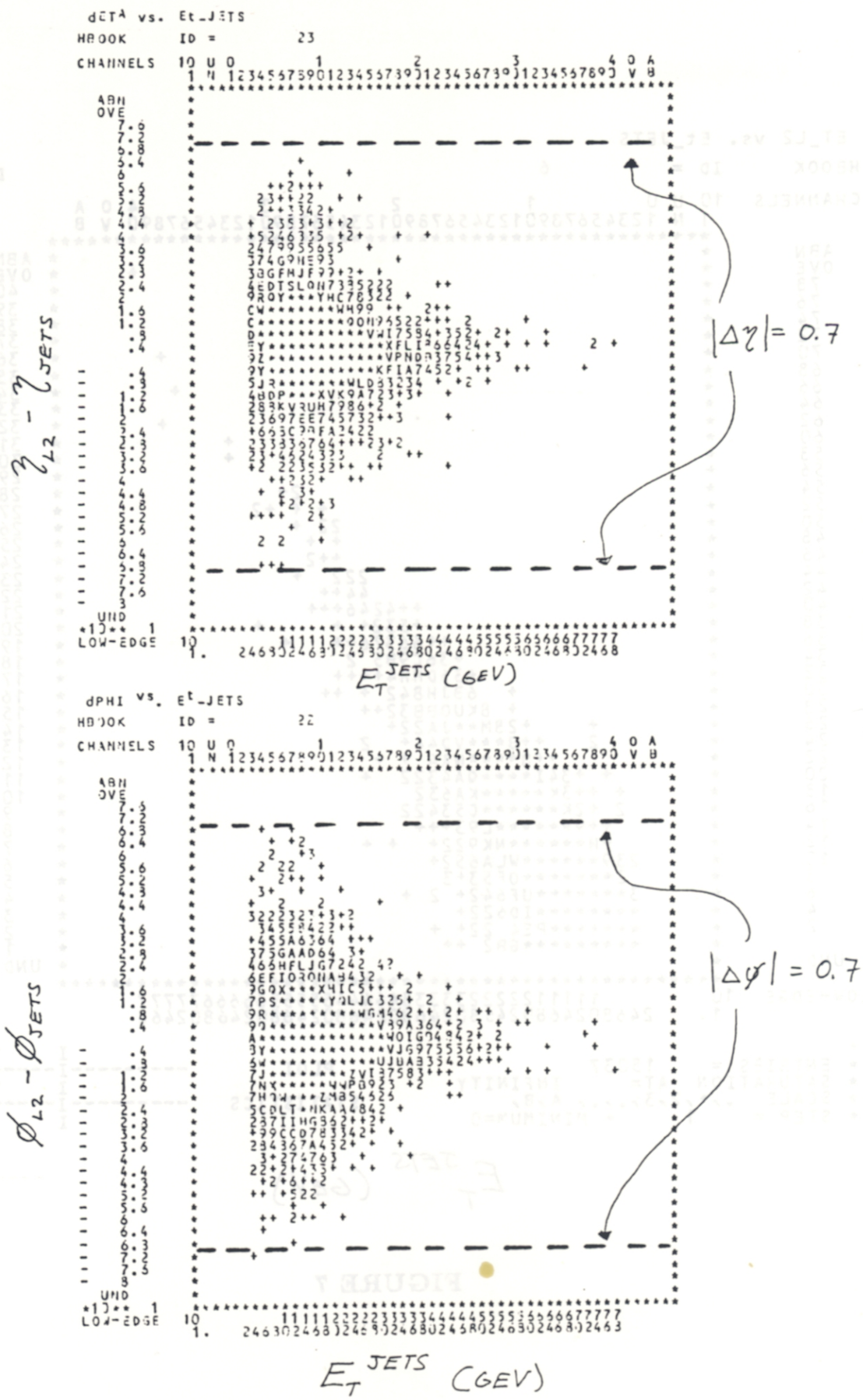
dETA vs. Et_JETS
HBOOK ID = 23
CHANNELS
$\eta_{L2} - \eta_{JETS}$
$|\Delta\eta| = 0.7$
E_T^{JETS} (GEV)
dPHI vs. Et_JETS
HBOOK ID = 22
CHANNELS
$\phi_{L2} - \phi_{JETS}$
$|\Delta\phi| = 0.7$
E_T^{JETS} (GEV)

FIGURE 6

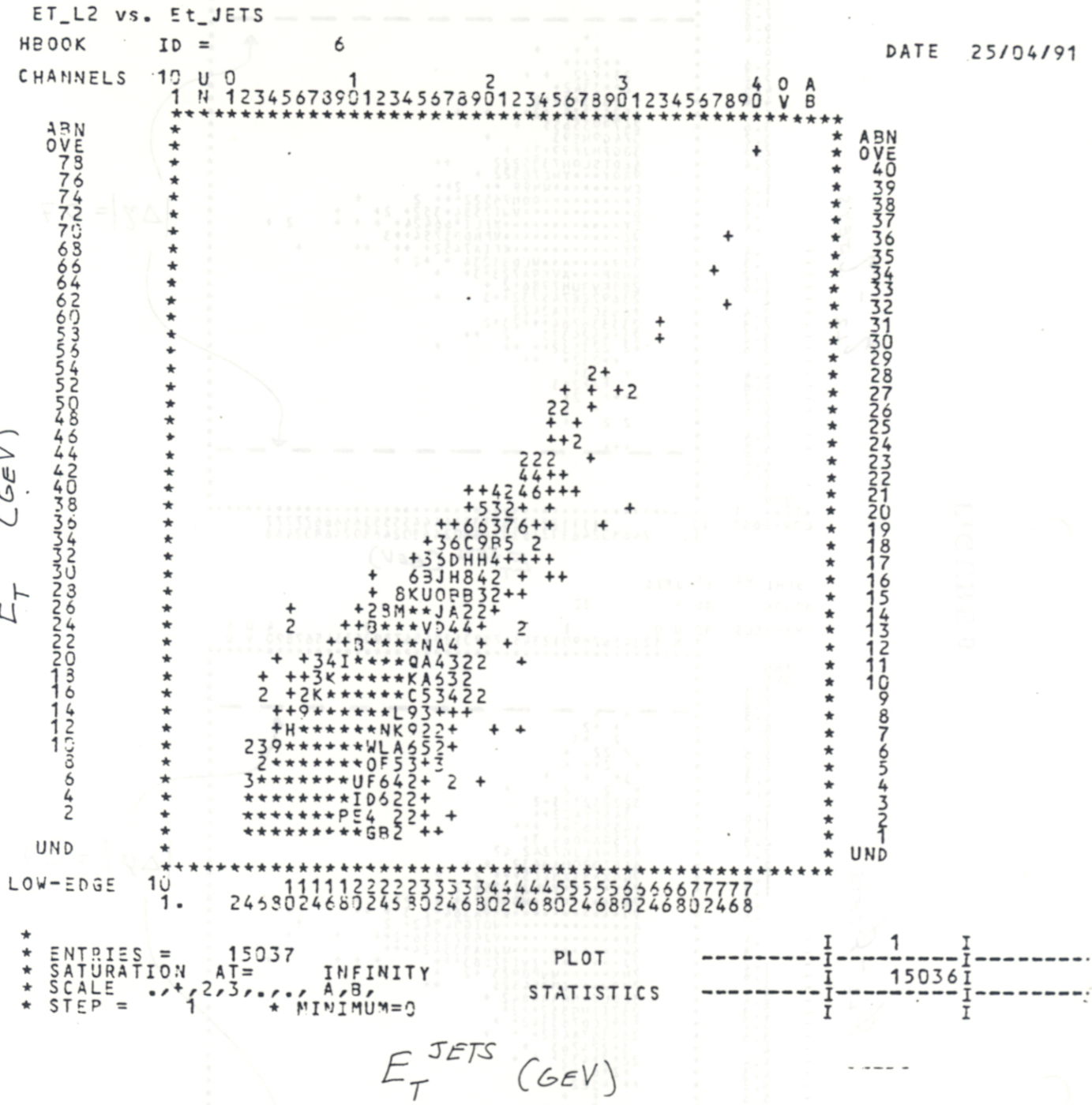
ET_L2 vs. Et_JETS
HBOOK ID = 6
DATE 25/04/91
CHANNELS
ABN
OVE
UND
LOW-EDGE
E_T^{L2} (GeV)
E_T^{JETS} (GEV)
ENTRIES = 15037
SATURATION AT= INFINITY
SCALE
STEP = 1
MINIMUM=0
PLOT
STATISTICS
1
15036

FIGURE 7

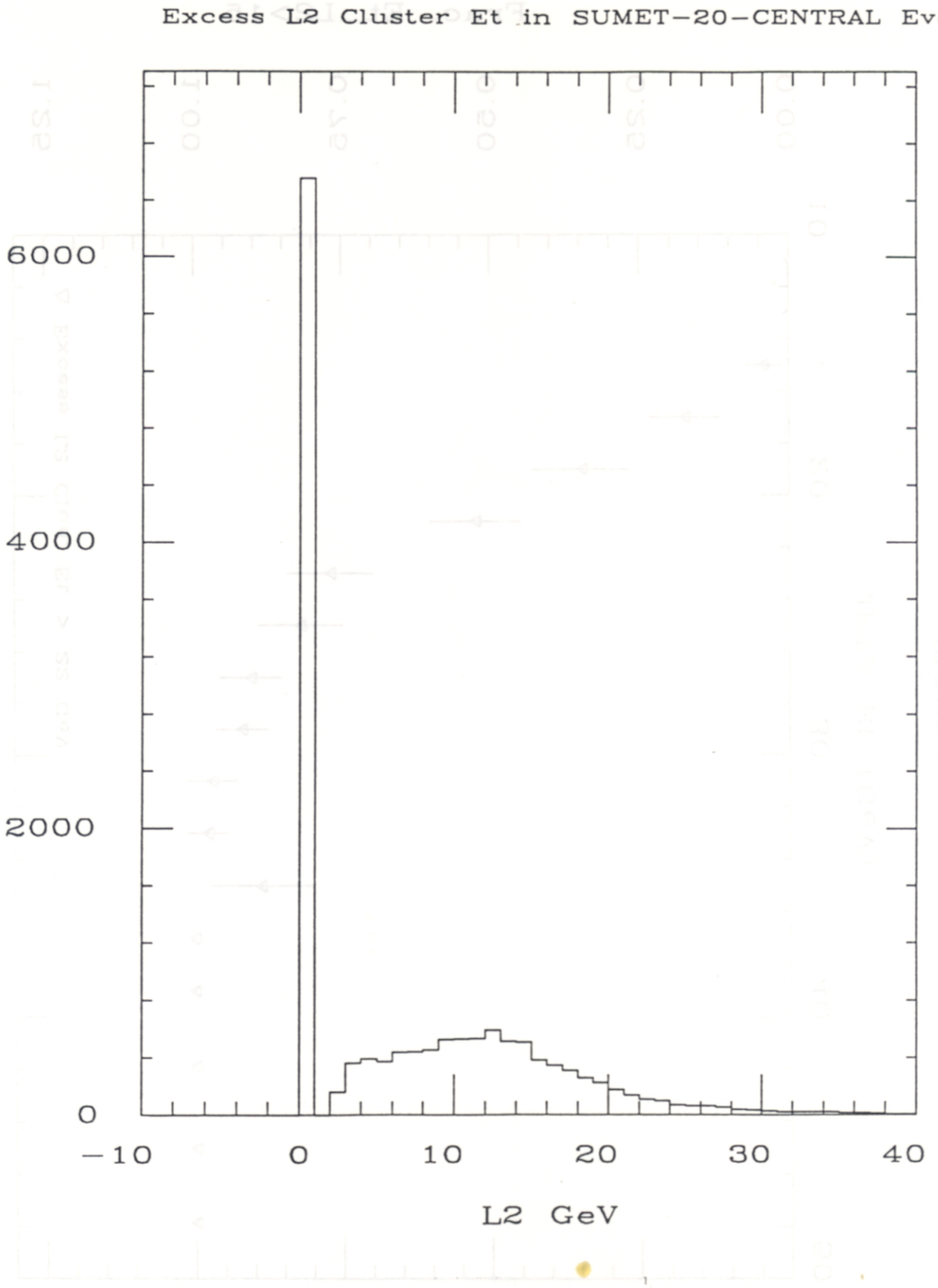
Excess L2 Cluster Et in SUMET-20-CENTRAL Events
6000
4000
2000
0
-10
0
10
20
30
40
L2 GeV

FIGURE 8

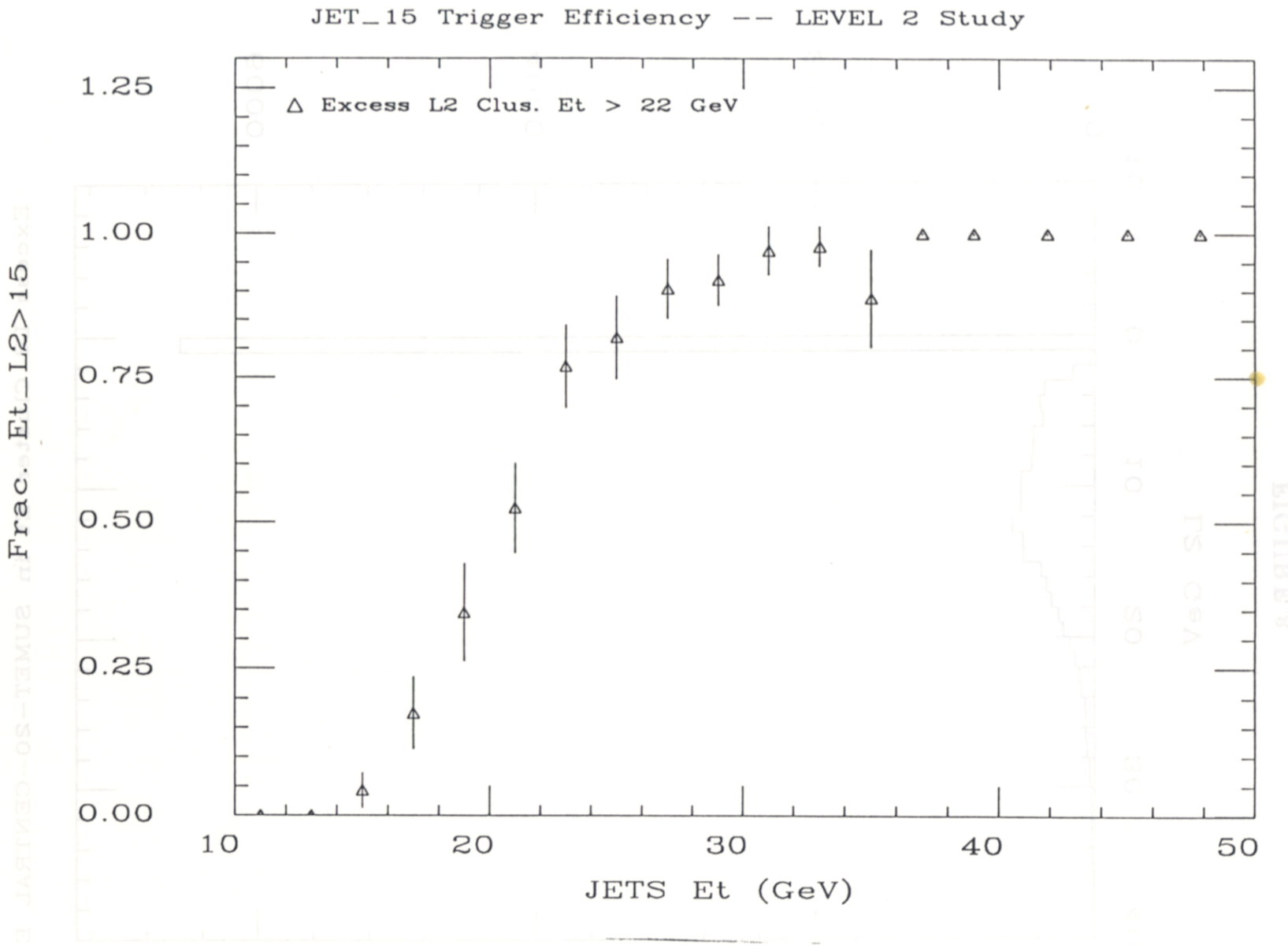
JET_15 Trigger Efficiency -- LEVEL 2 Study
Δ Excess L2 Clus. Et > 22 GeV
Frac. Et_L2>15
1.25
1.00
0.75
0.50
0.25
0.00
10
20
30
40
50
JETS Et (GeV)

FIGURE 9

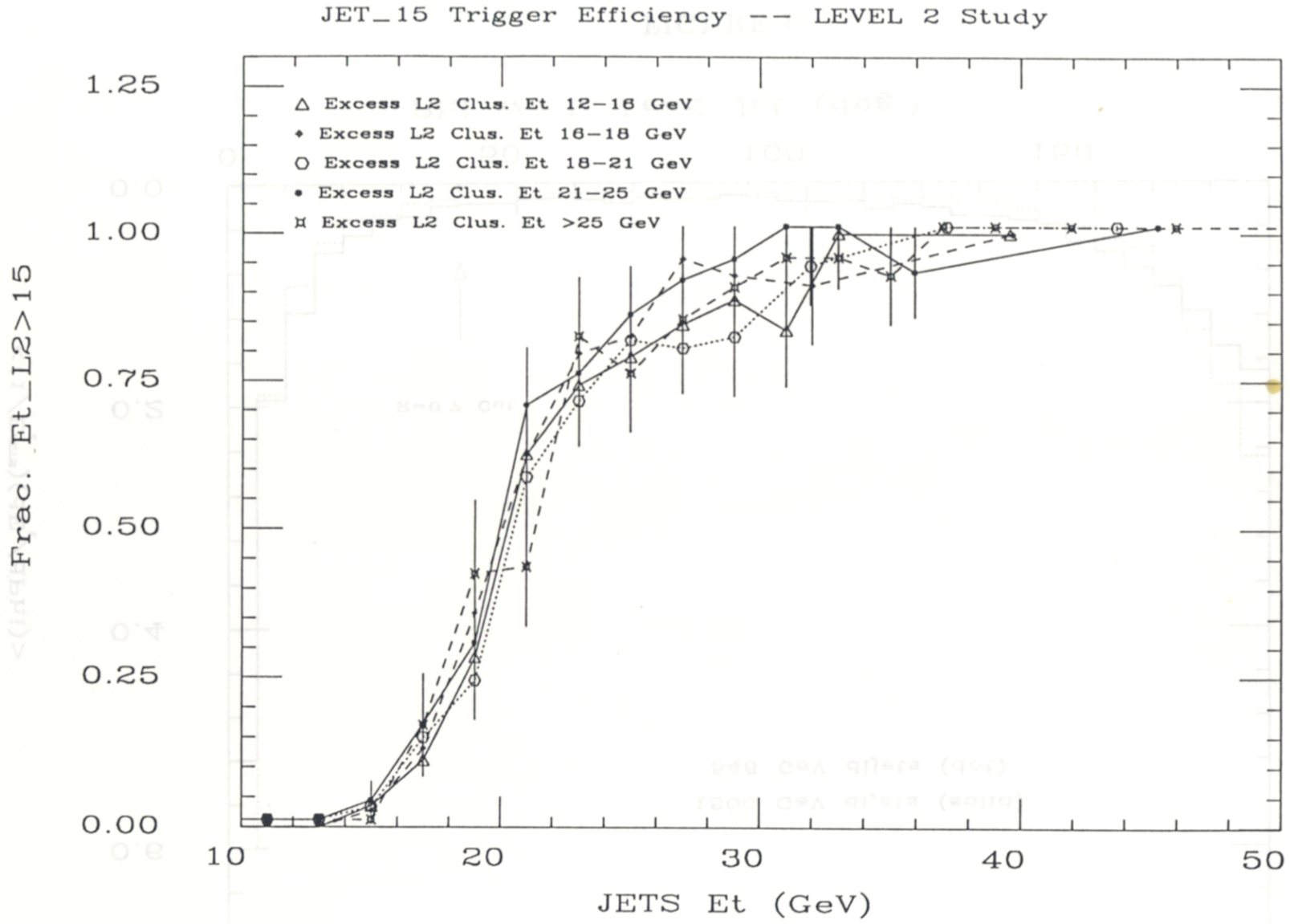
JET_15 Trigger Efficiency -- LEVEL 2 Study
Excess L2 Clus. Et 12-16 GeV
Excess L2 Clus. Et 16-18 GeV
Excess L2 Clus. Et 18-21 GeV
Excess L2 Clus. Et 21-25 GeV
Excess L2 Clus. Et >25 GeV
Frac. Et_L2>15
1.25
1.00
0.75
0.50
0.25
0.00
10
20
30
40
50
JETS Et (GeV)

FIGURE 10

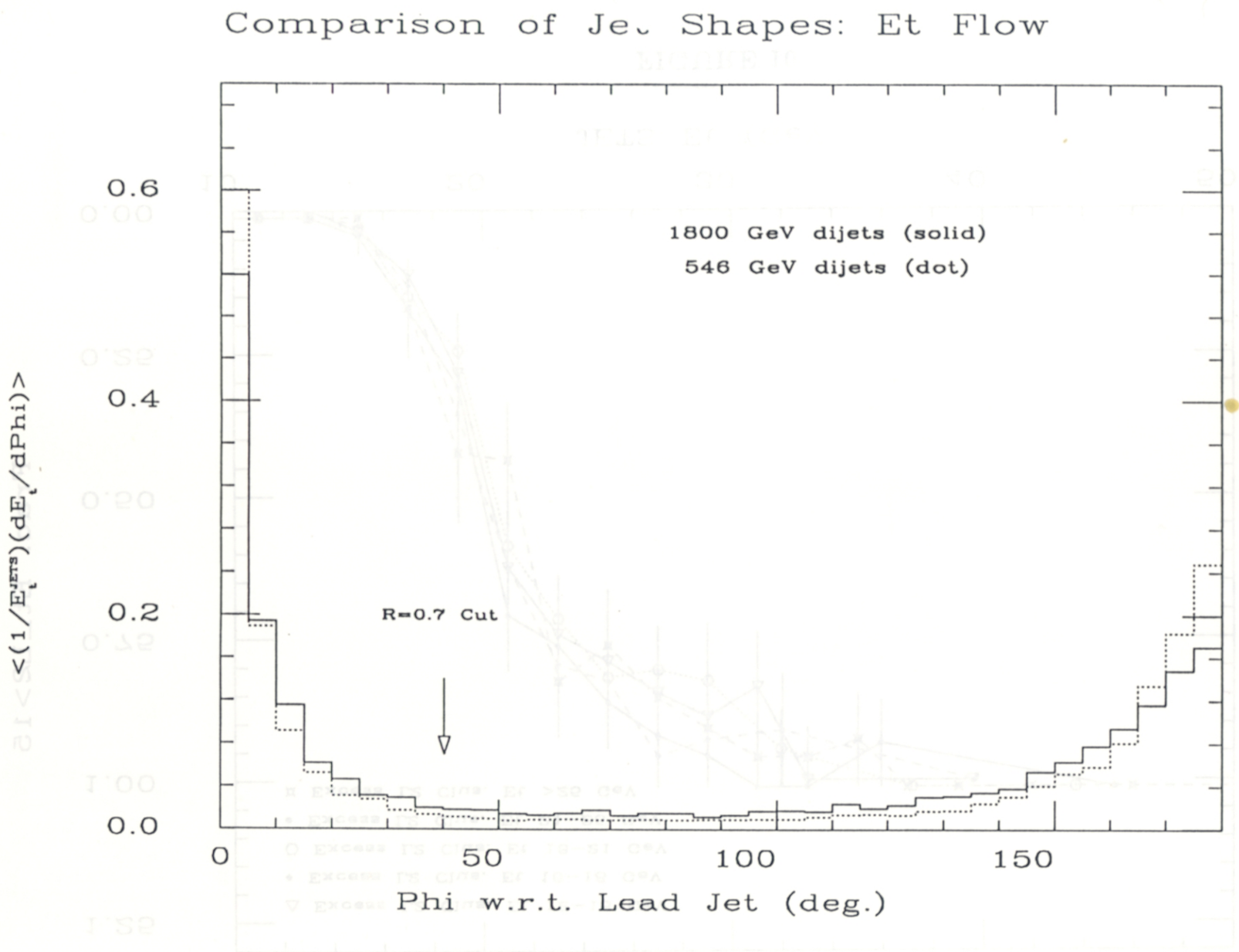
Comparison of Jet Shapes: Et Flow
1800 GeV dijets (solid)
546 GeV dijets (dot)
R=0.7 Cut
<(1/E_t^JETS)(dE_t/dPhi)>
0.0
0.2
0.4
0.6
0
50
100
150
Phi w.r.t. Lead Jet (deg.)

FIGURE 11

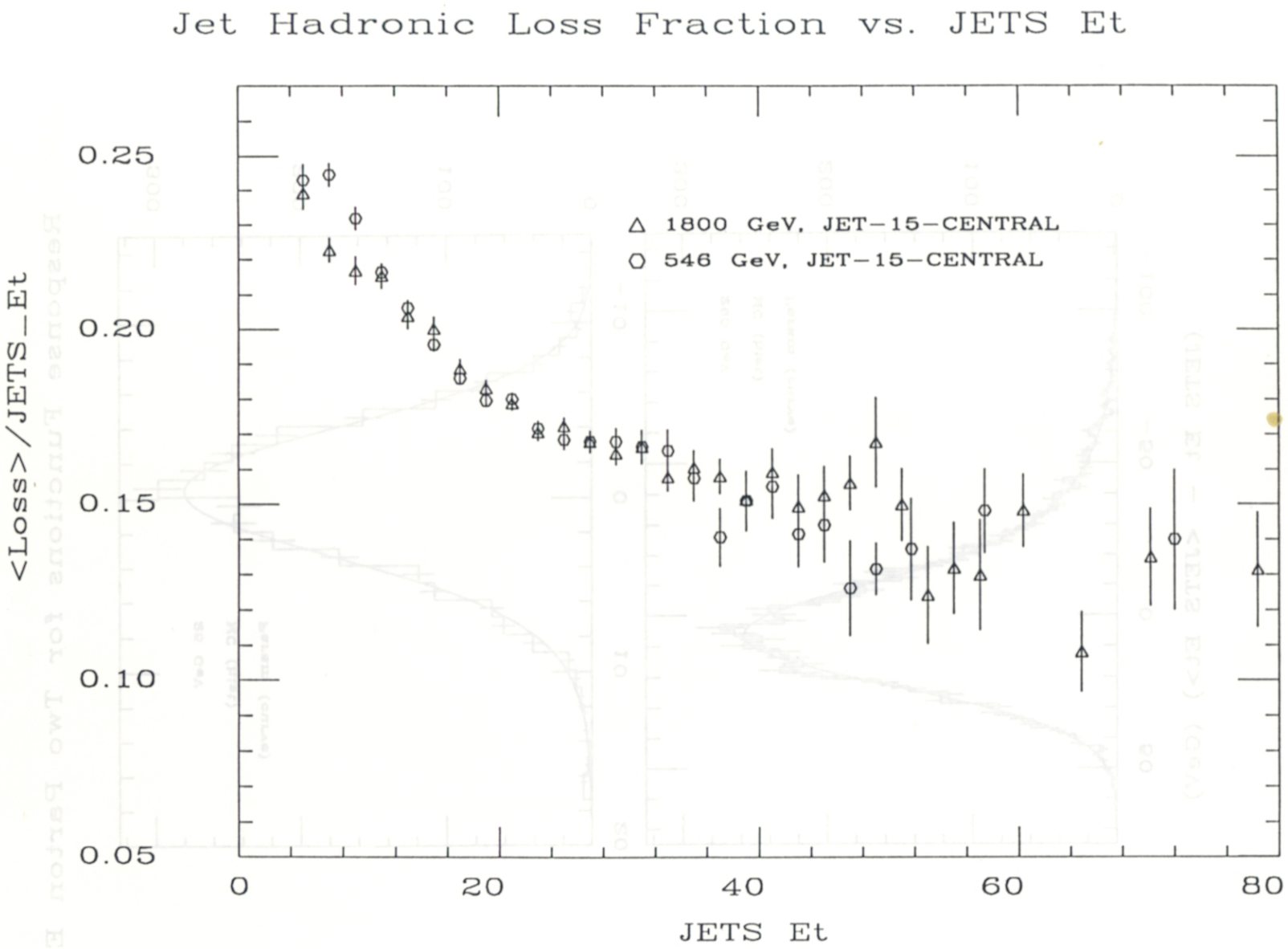
Jet Hadronic Loss Fraction vs. JETS Et
<Loss>/JETS_Et
0.25
0.20
0.15
0.10
0.05
0
20
40
60
80
JETS Et
1800 GeV, JET-15-CENTRAL
546 GeV, JET-15-CENTRAL

FIGURE 12

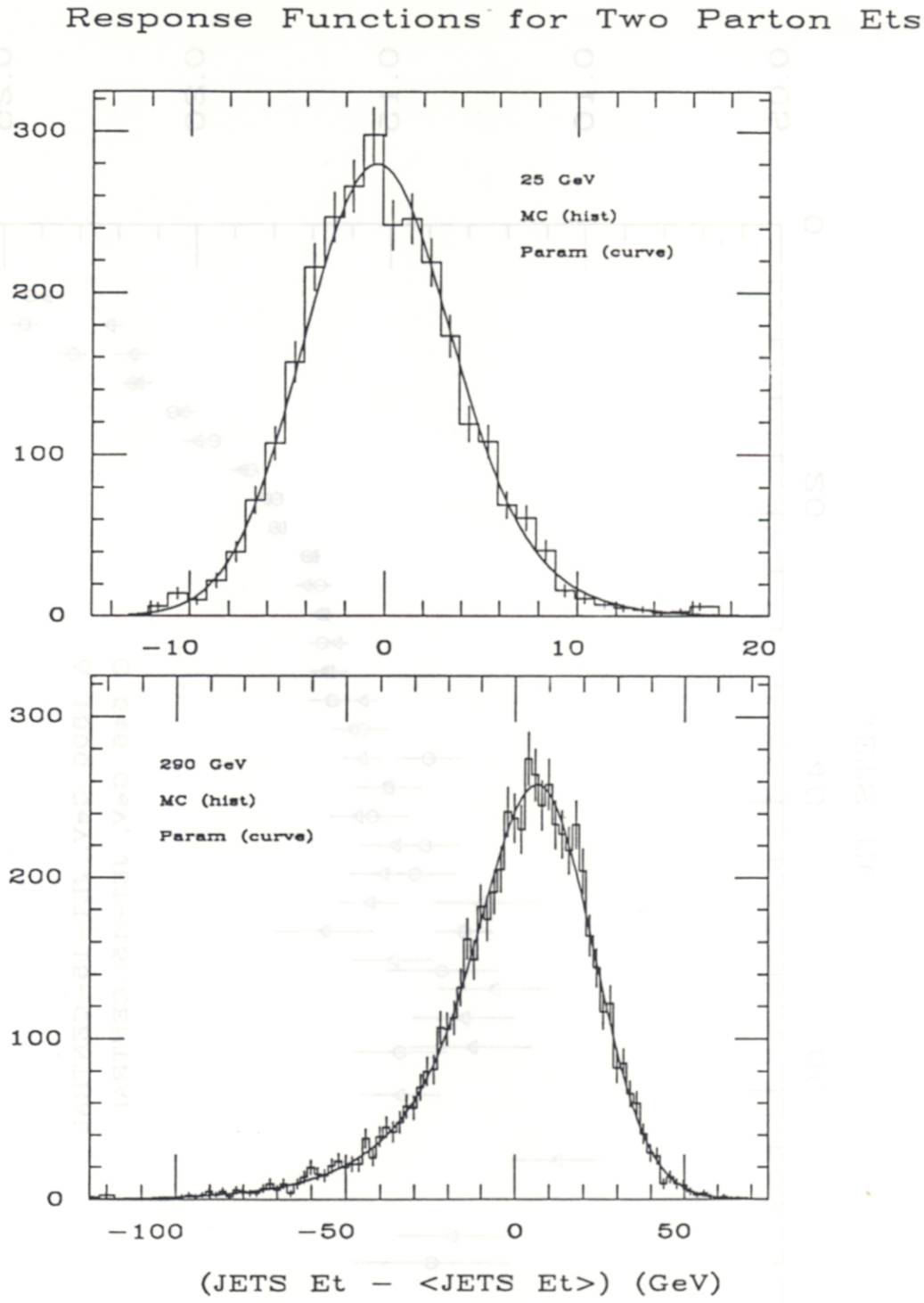
Response Functions for Two Parton Ets
300
200
100
0
25 GeV
MC (hist)
Param (curve)
−10
0
10
20
300
200
100
0
290 GeV
MC (hist)
Param (curve)
−100
−50
0
50
(JETS Et − <JETS Et>) (GeV)

FIGURE 13

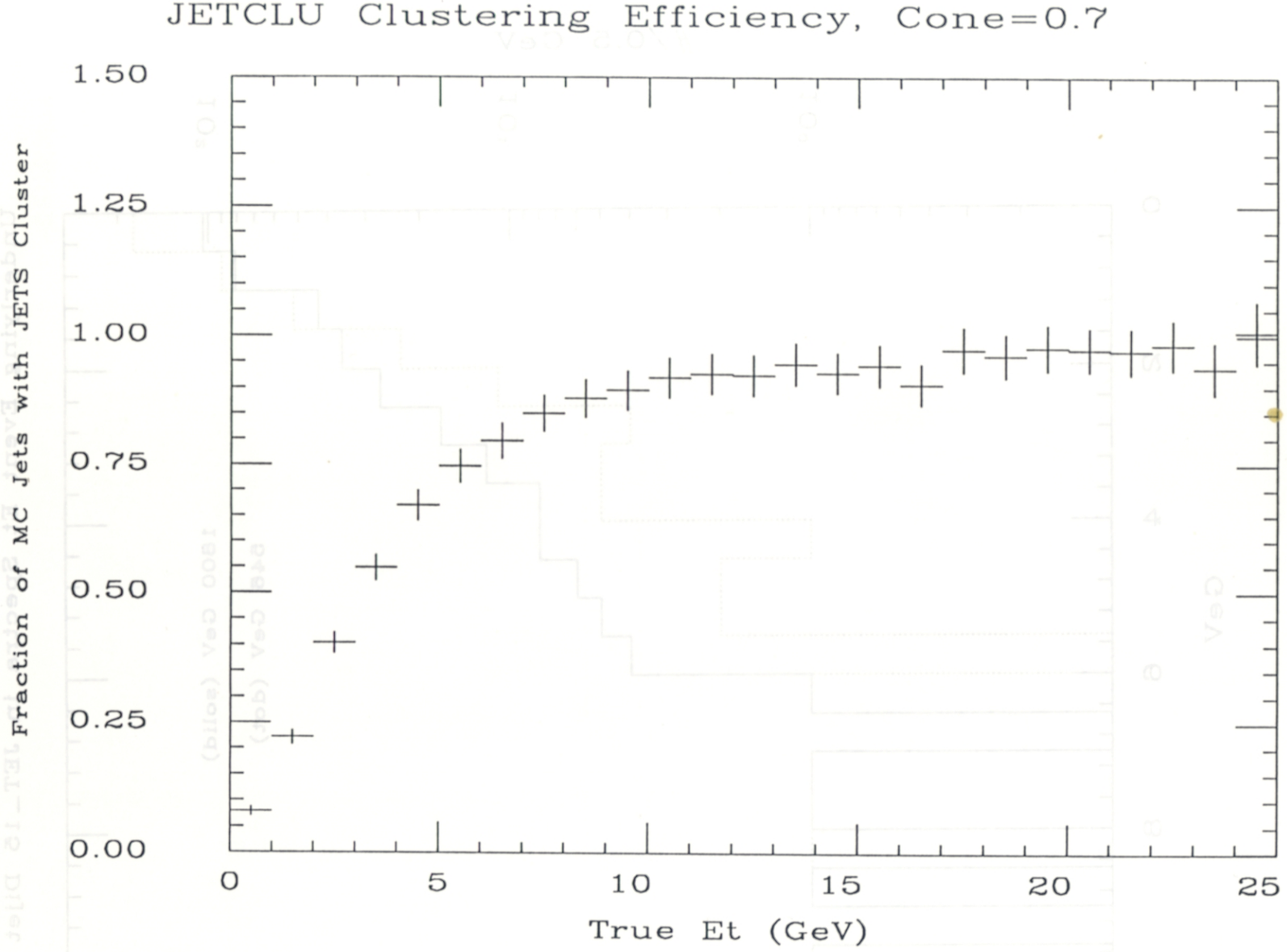
JETCLU Clustering Efficiency, Cone=0.7
Fraction of MC Jets with JETS Cluster
1.50
1.25
1.00
0.75
0.50
0.25
0.00
0
5
10
15
20
25
True Et (GeV)

FIGURE 14

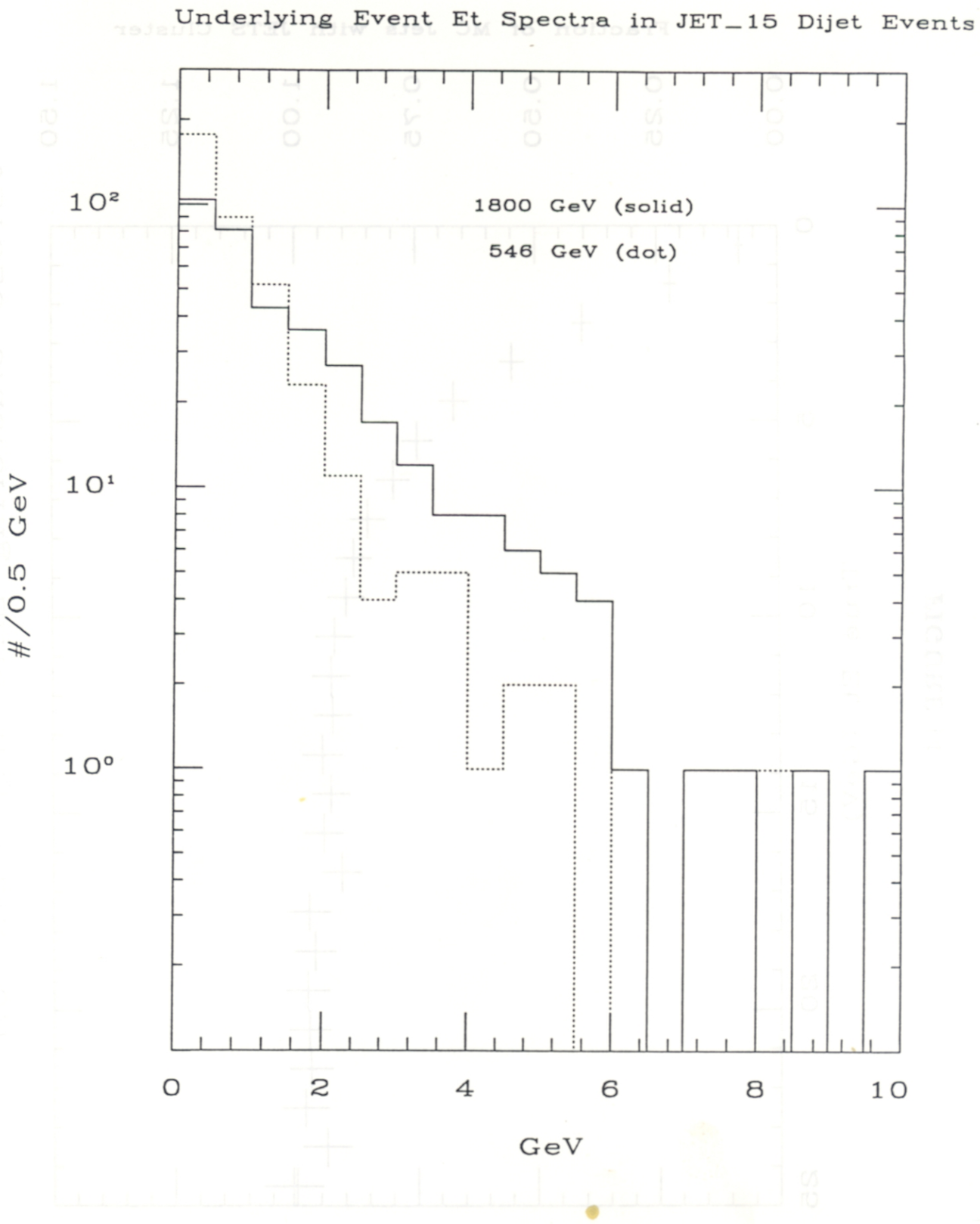
Underlying Event Et Spectra in JET_15 Dijet Events
1800 GeV (solid)
546 GeV (dot)
#/0.5 GeV
10²
10¹
10°
0
2
4
6
8
10
GeV

FIGURE 15

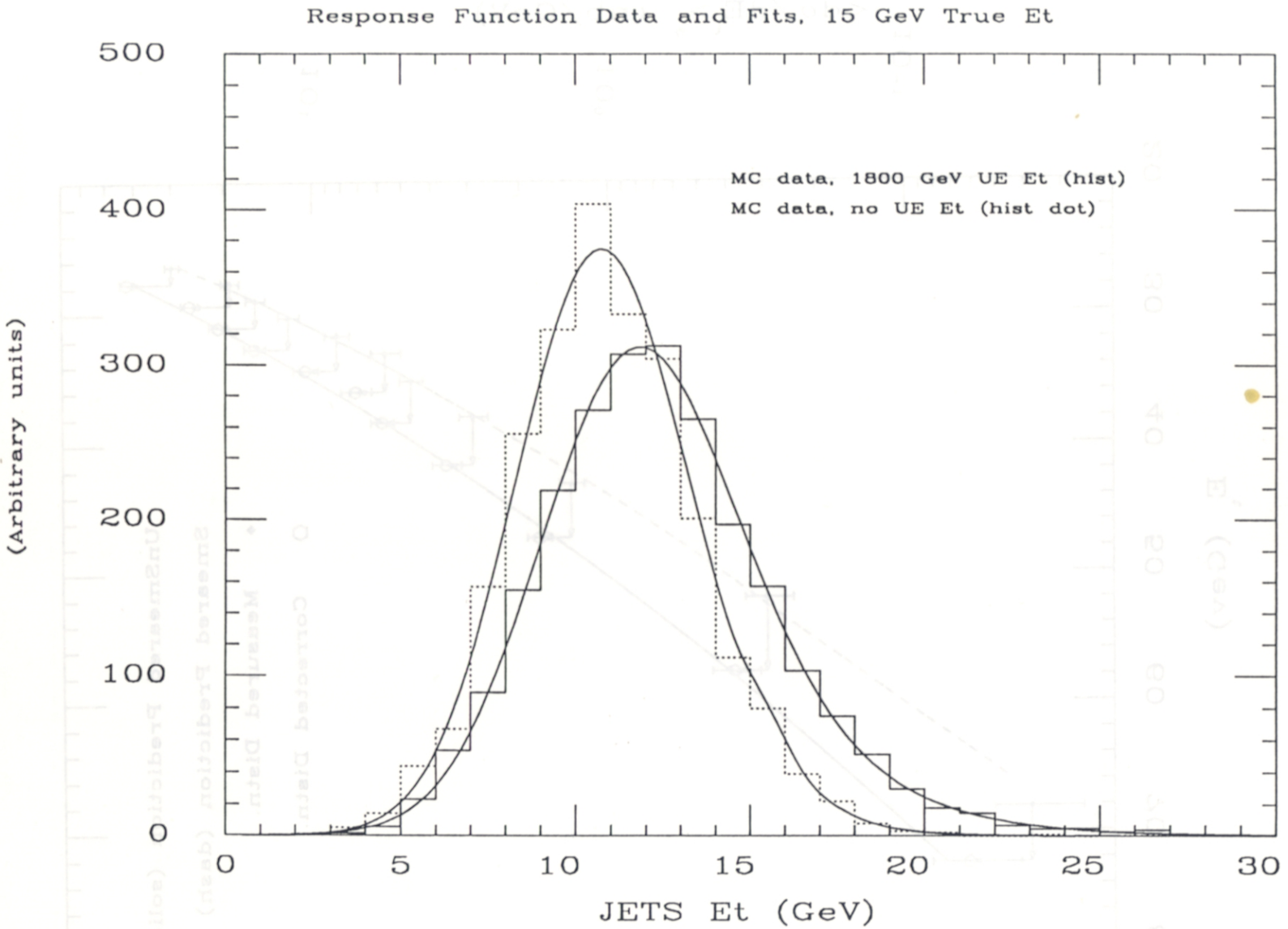
Response Function Data and Fits, 15 GeV True Et
MC data, 1800 GeV UE Et (hist)
MC data, no UE Et (hist dot)
(Arbitrary units)
JETS Et (GeV)
0
100
200
300
400
500
0
5
10
15
20
25
30

FIGURE 16

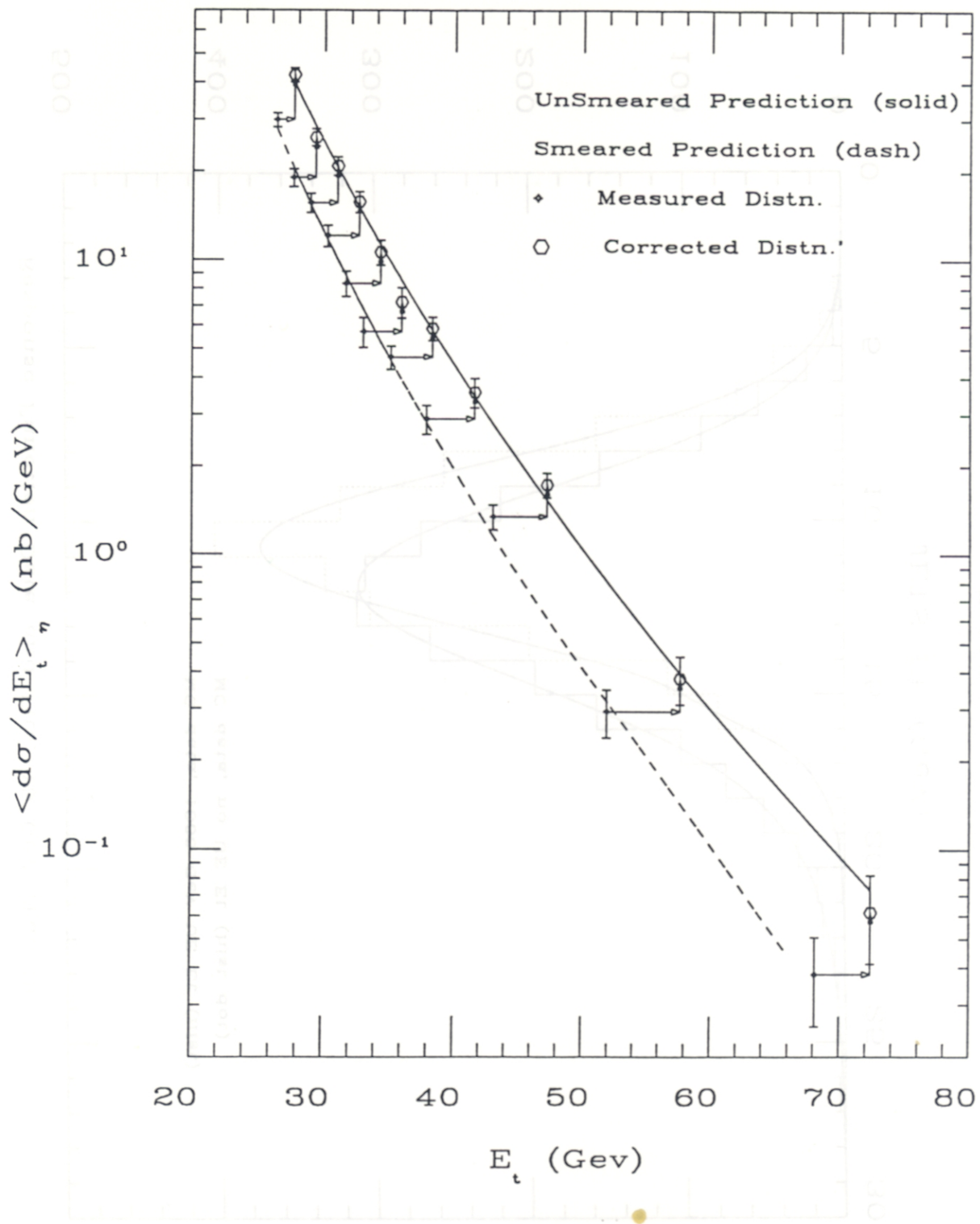
Smearing Corrections at 546 GeV
UnSmeared Prediction (solid)
Smeared Prediction (dash)
Measured Distn.
Corrected Distn.'
10^1
10^0
10^{-1}
$<d\sigma/dE_t>_\eta$ (nb/GeV)
20
30
40
50
60
70
80
E_t (Gev)

FIGURE 17

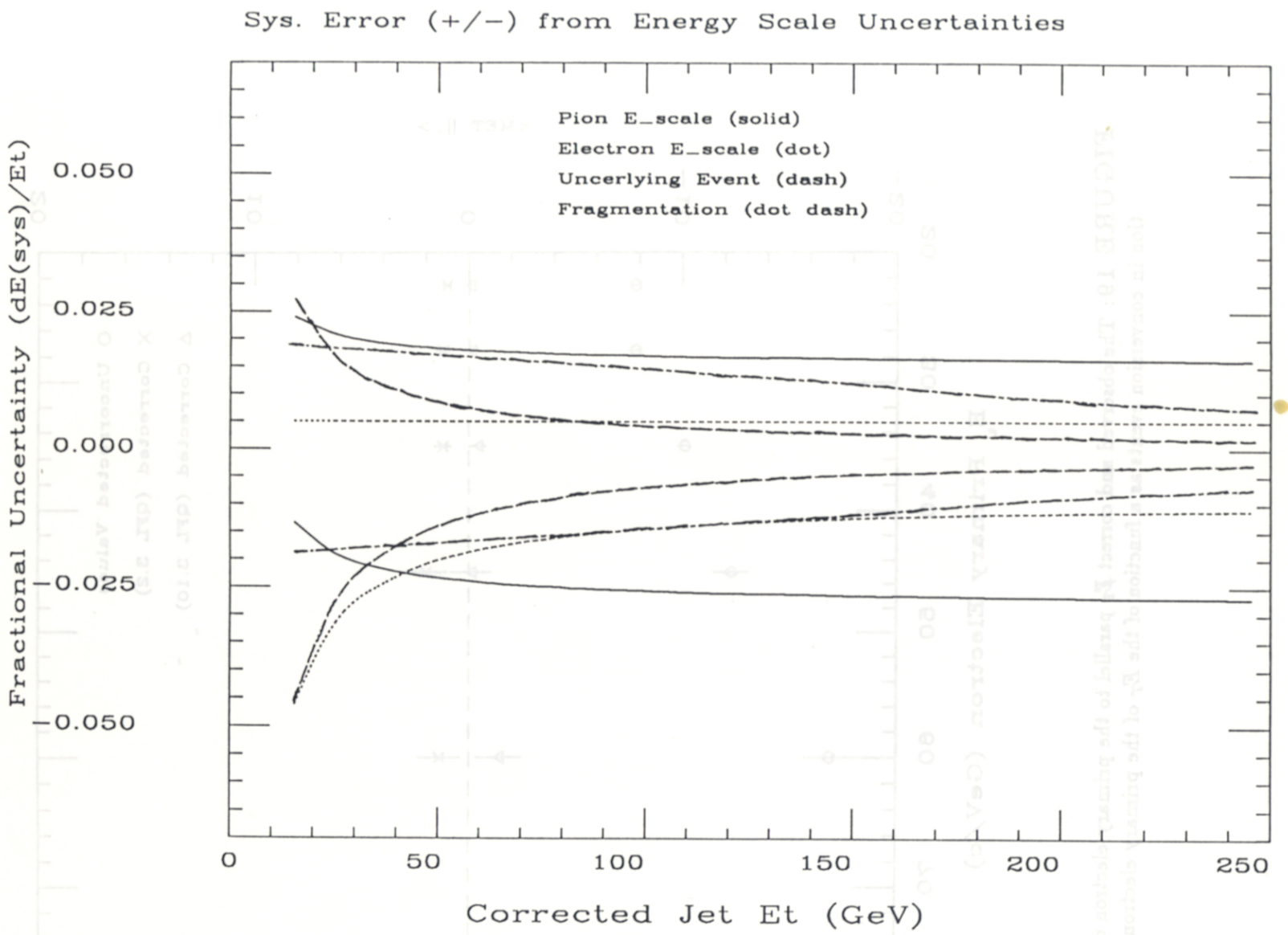
Sys. Error (+/−) from Energy Scale Uncertainties
Pion E_scale (solid)
Electron E_scale (dot)
Uncerlying Event (dash)
Fragmentation (dot dash)
Fractional Uncertainty (dE(sys)/Et)
0.050
0.025
0.000
−0.025
−0.050
0
50
100
150
200
250
Corrected Jet Et (GeV)

FIGURE 18

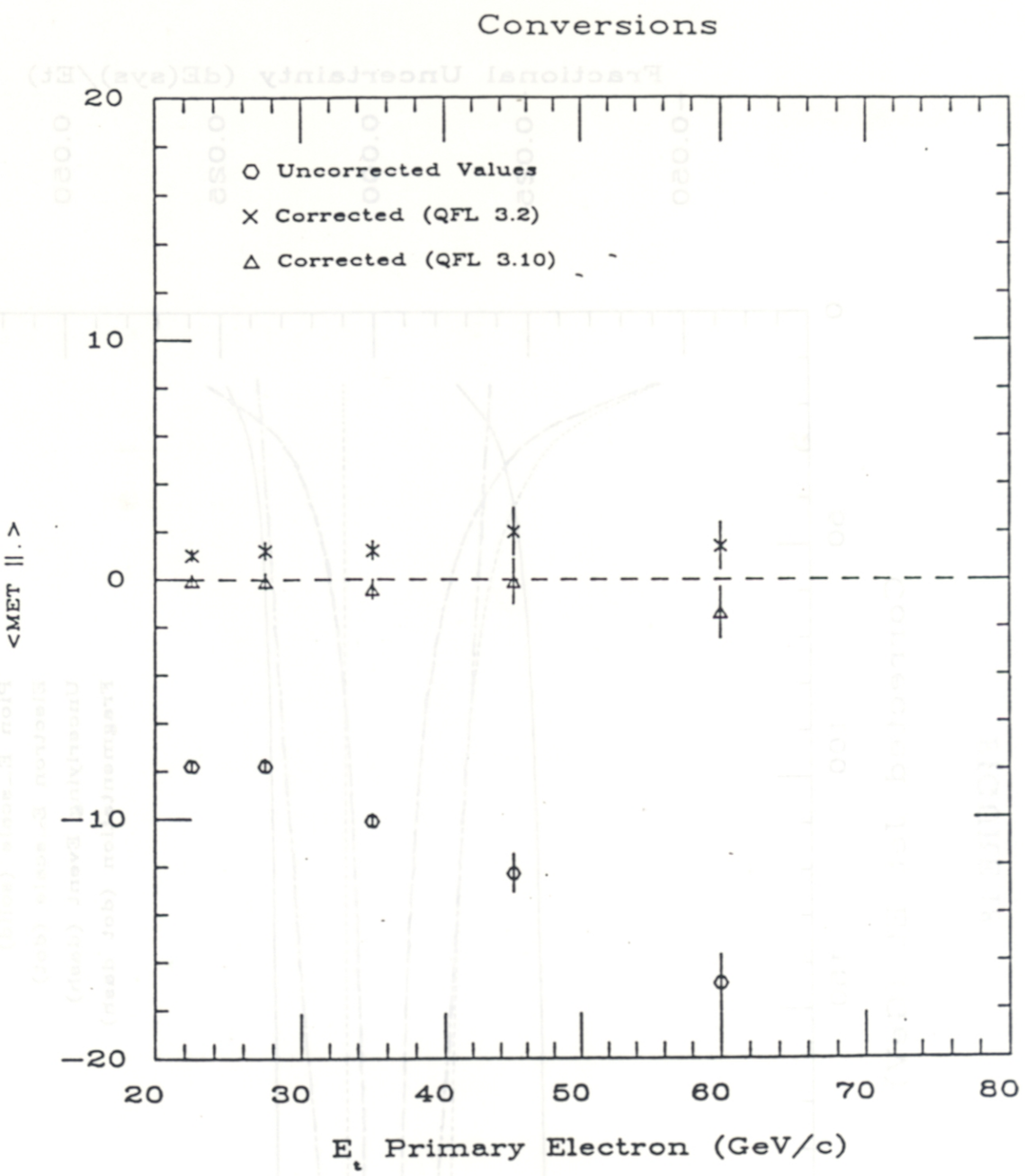

FIGURE 19: The observed and correct $\not\!\!E_T$ parallel to the primary electron direction in conversion events as a function of the E_T of the primary electron.

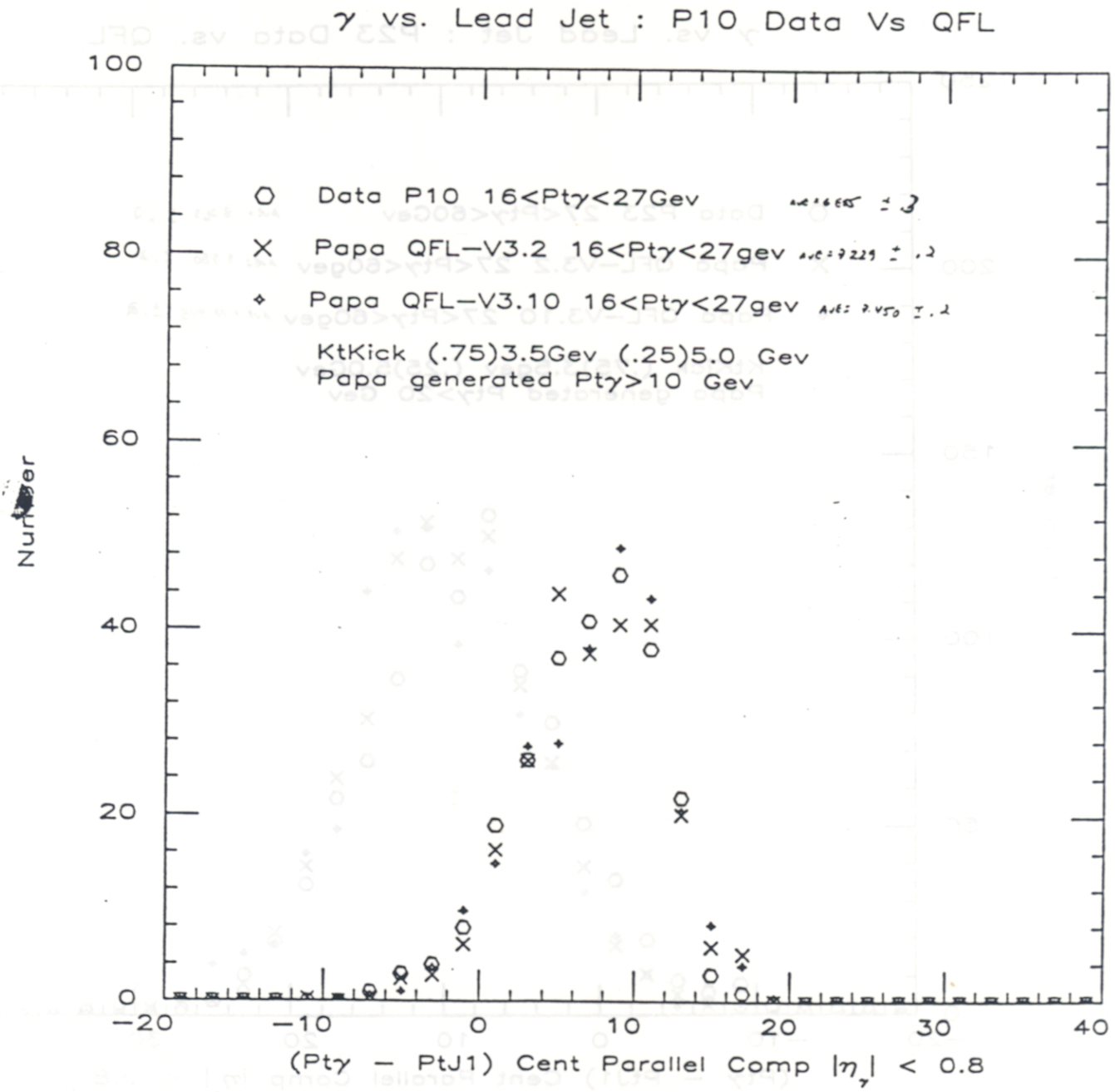
γ vs. Lead Jet : P10 Data Vs QFL
Data P10 16<Ptγ<27Gev
Papa QFL—V3.2 16<Ptγ<27gev
Papa QFL—V3.10 16<Ptγ<27gev
KtKick (.75)3.5Gev (.25)5.0 Gev
Papa generated Ptγ>10 Gev
Number
100
80
60
40
20
0
−20
−10
0
10
20
30
40
(Ptγ − PtJ1) Cent Parallel Comp |η_γ| < 0.8

FIGURE 20

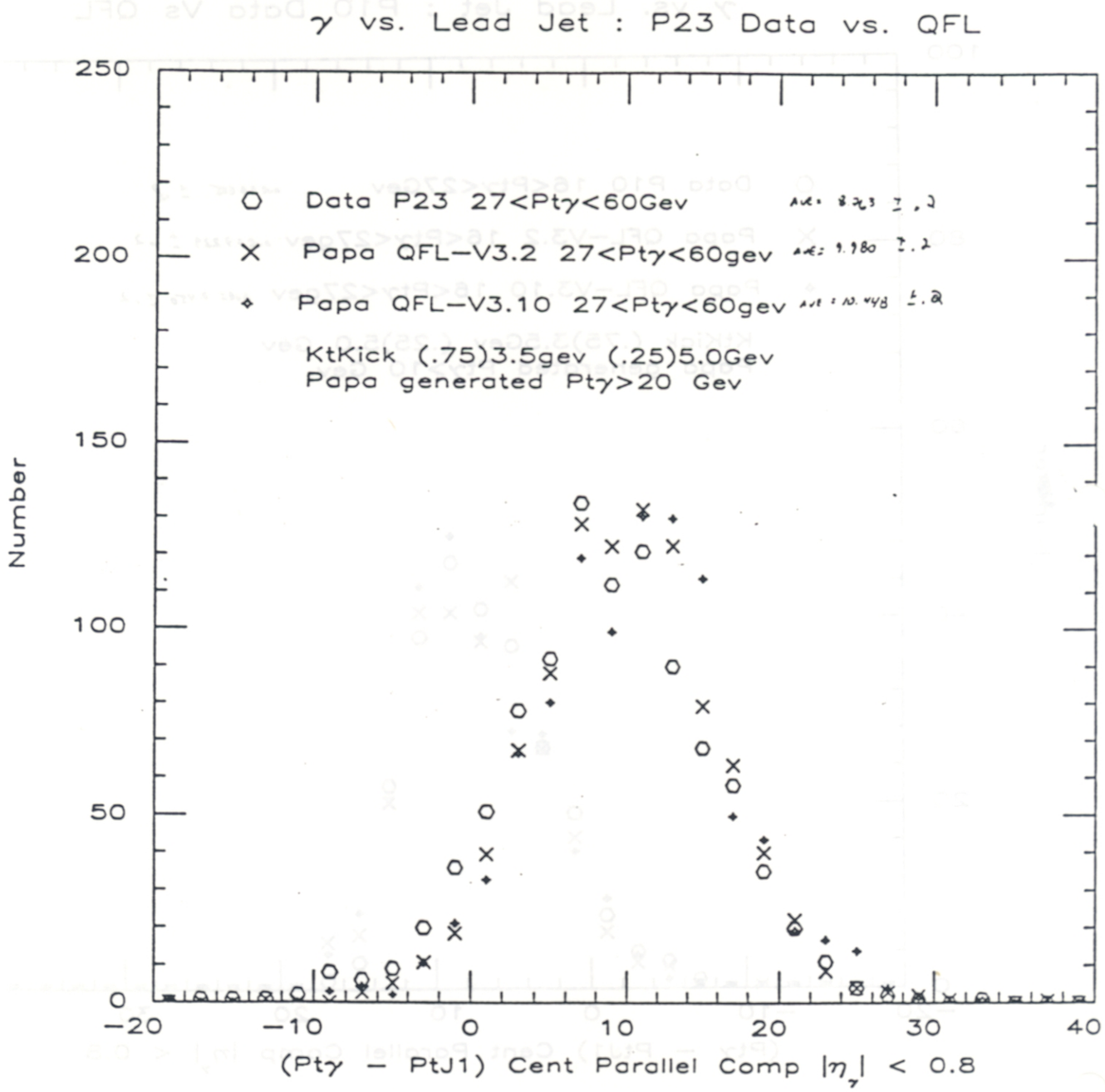
γ vs. Lead Jet : P23 Data vs. QFL
Data P23 27<Ptγ<60Gev
Papa QFL—V3.2 27<Ptγ<60gev
Papa QFL—V3.10 27<Ptγ<60gev
KtKick (.75)3.5gev (.25)5.0Gev
Papa generated Ptγ>20 Gev
Number
250
200
150
100
50
0
−20
−10
0
10
20
30
40
(Ptγ − PtJ1) Cent Parallel Comp |η_γ| < 0.8

FIGURE 21

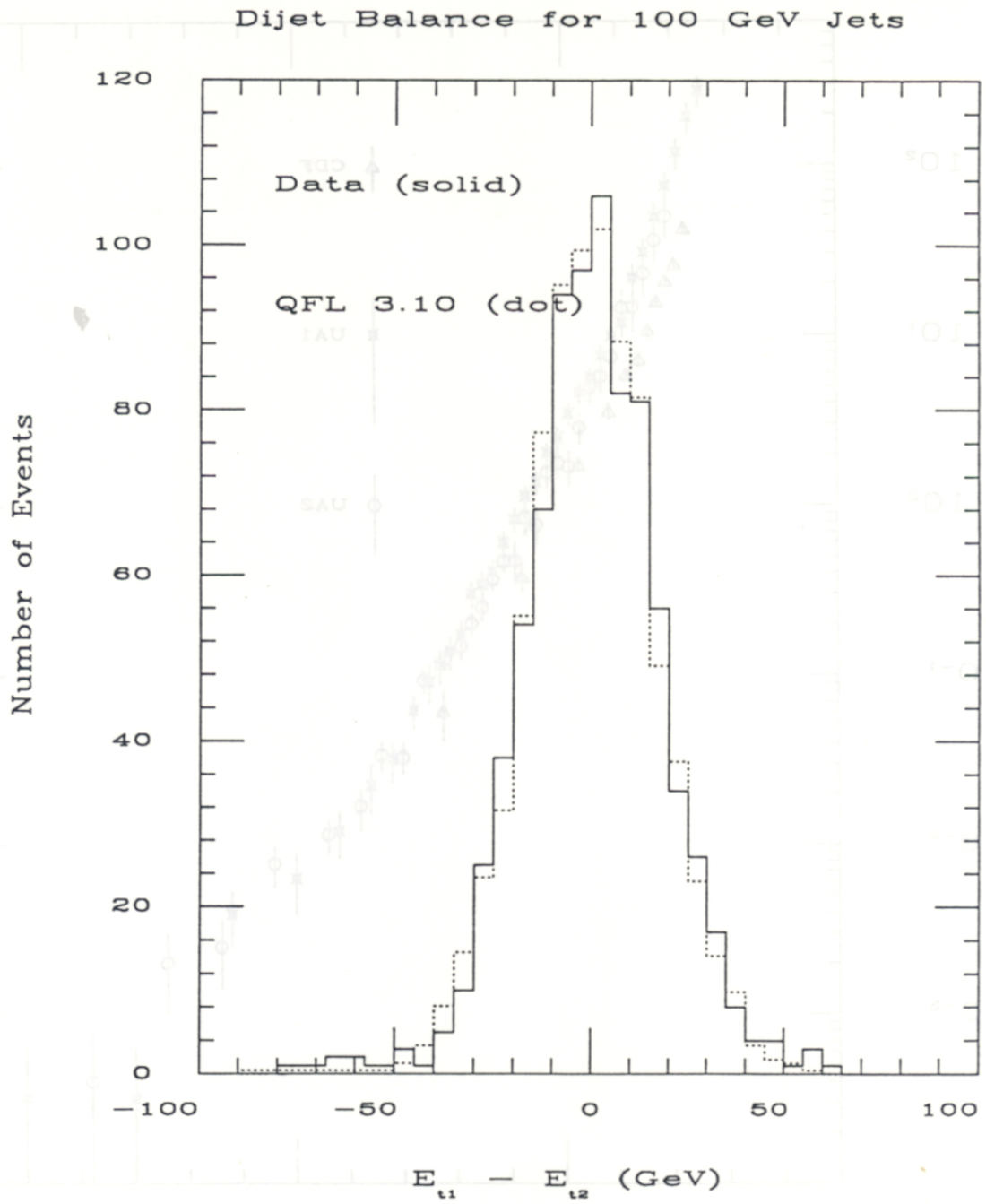
Dijet Balance for 100 GeV Jets
Data (solid)
QFL 3.10 (dot)
Number of Events
120
100
80
60
40
20
0
−100
−50
0
50
100
E_t1 − E_t2 (GeV)

FIGURE 22

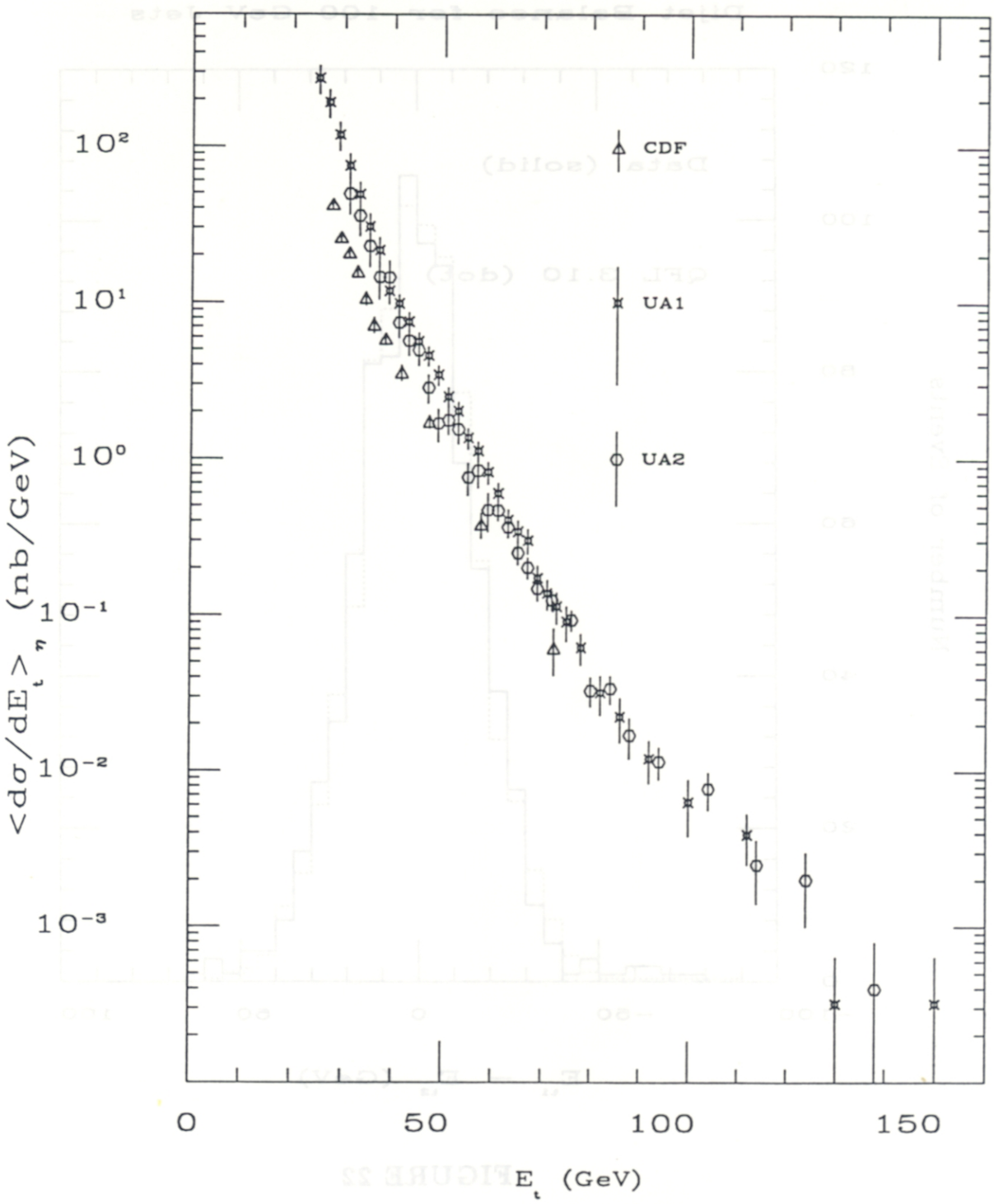
Inclusive Jet Cross Sections at 546 GeV
CDF
UA1
UA2
10^2
10^1
10^0
10^{-1}
10^{-2}
10^{-3}
$<d\sigma/dE_t>_\eta$ (nb/GeV)
0
50
100
150
E_t (GeV)

FIGURE 23

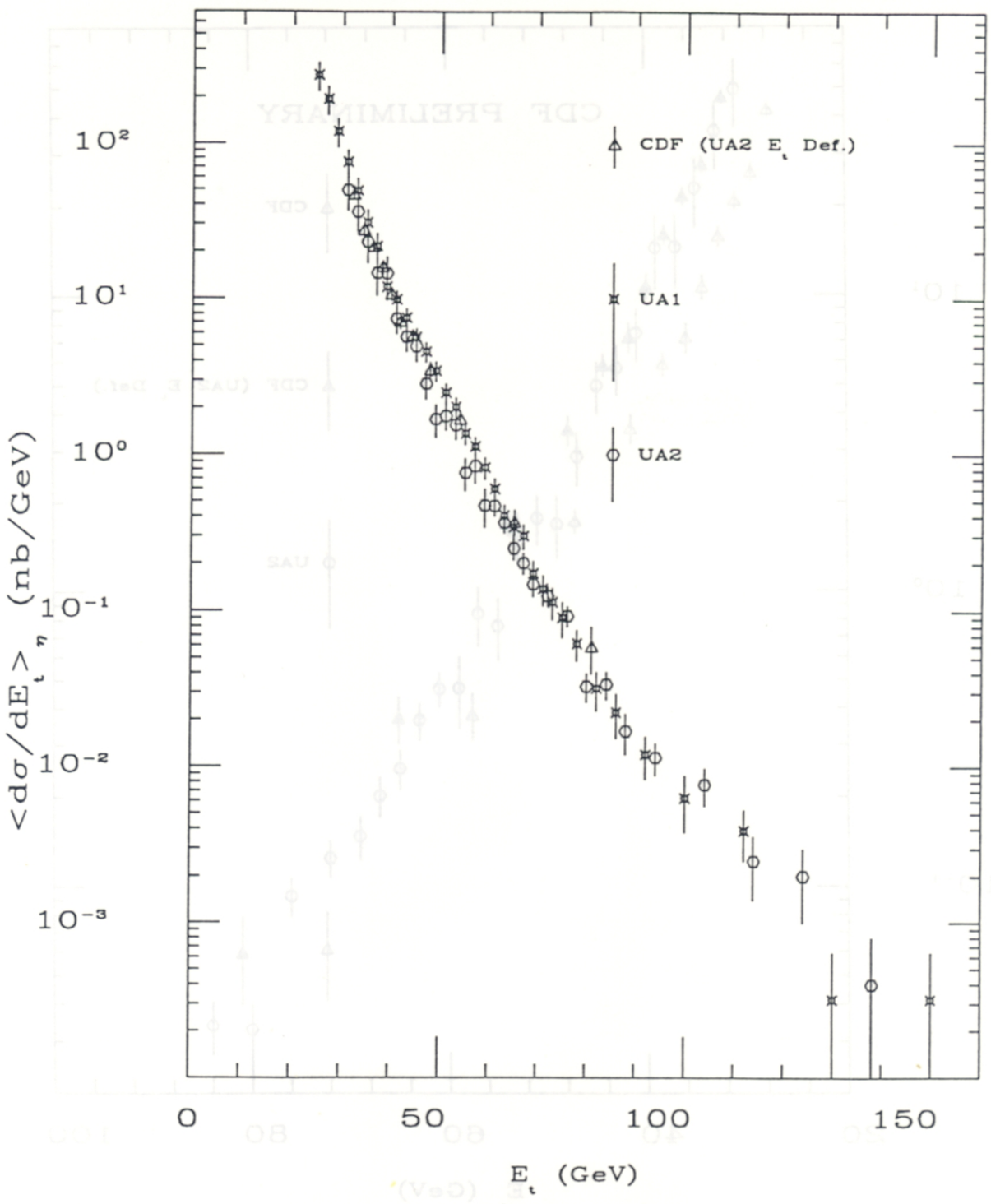
Inclusive Jet Cross Sections at 546 GeV
CDF (UA2 E_t Def.)
UA1
UA2
10²
10¹
10⁰
10⁻¹
10⁻²
10⁻³
<dσ/dE_t>_η (nb/GeV)
0
50
100
150
E_t (GeV)

FIGURE 24

Inclusive Jet Cross Sections at 546 GeV

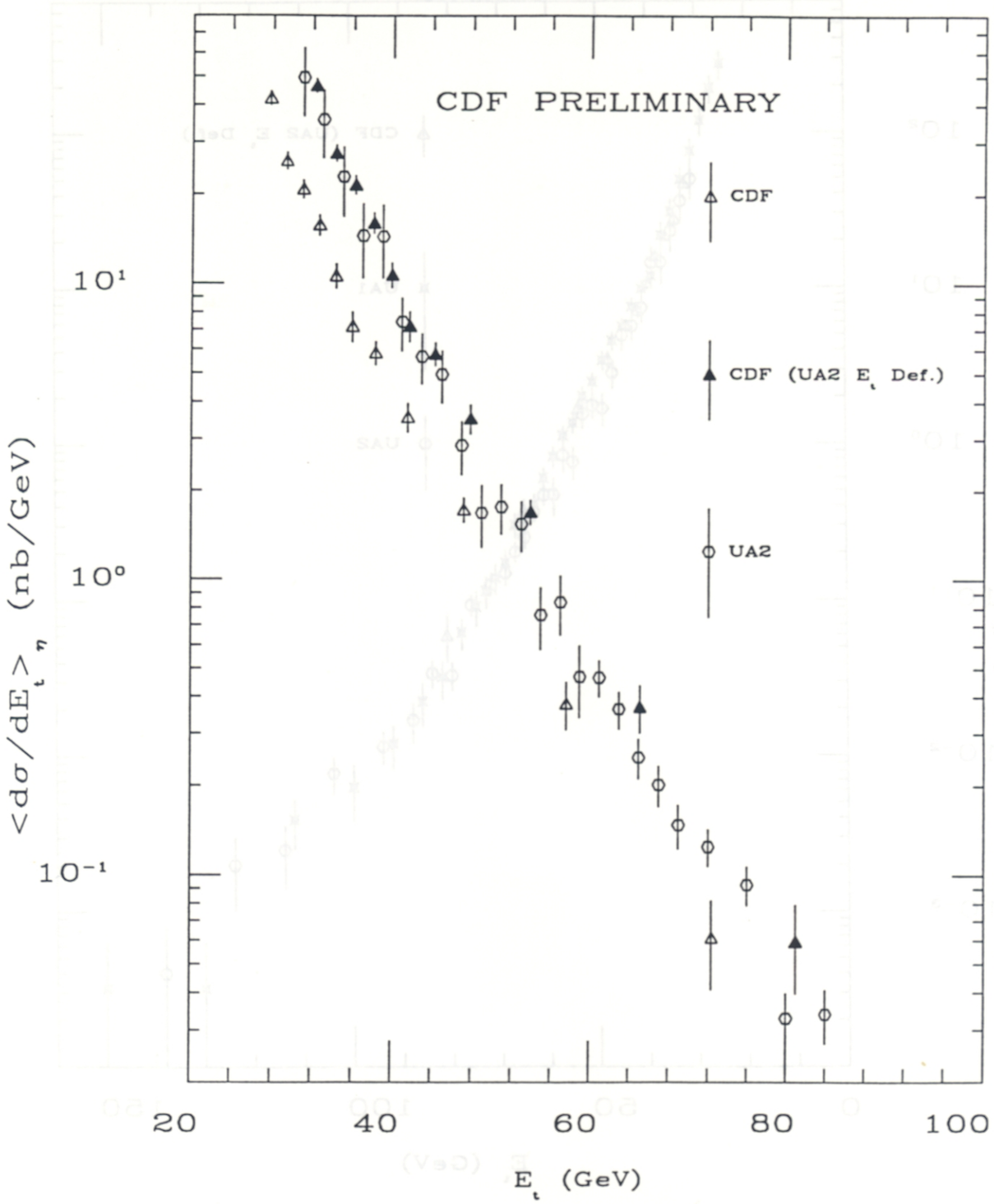

FIGURE 25

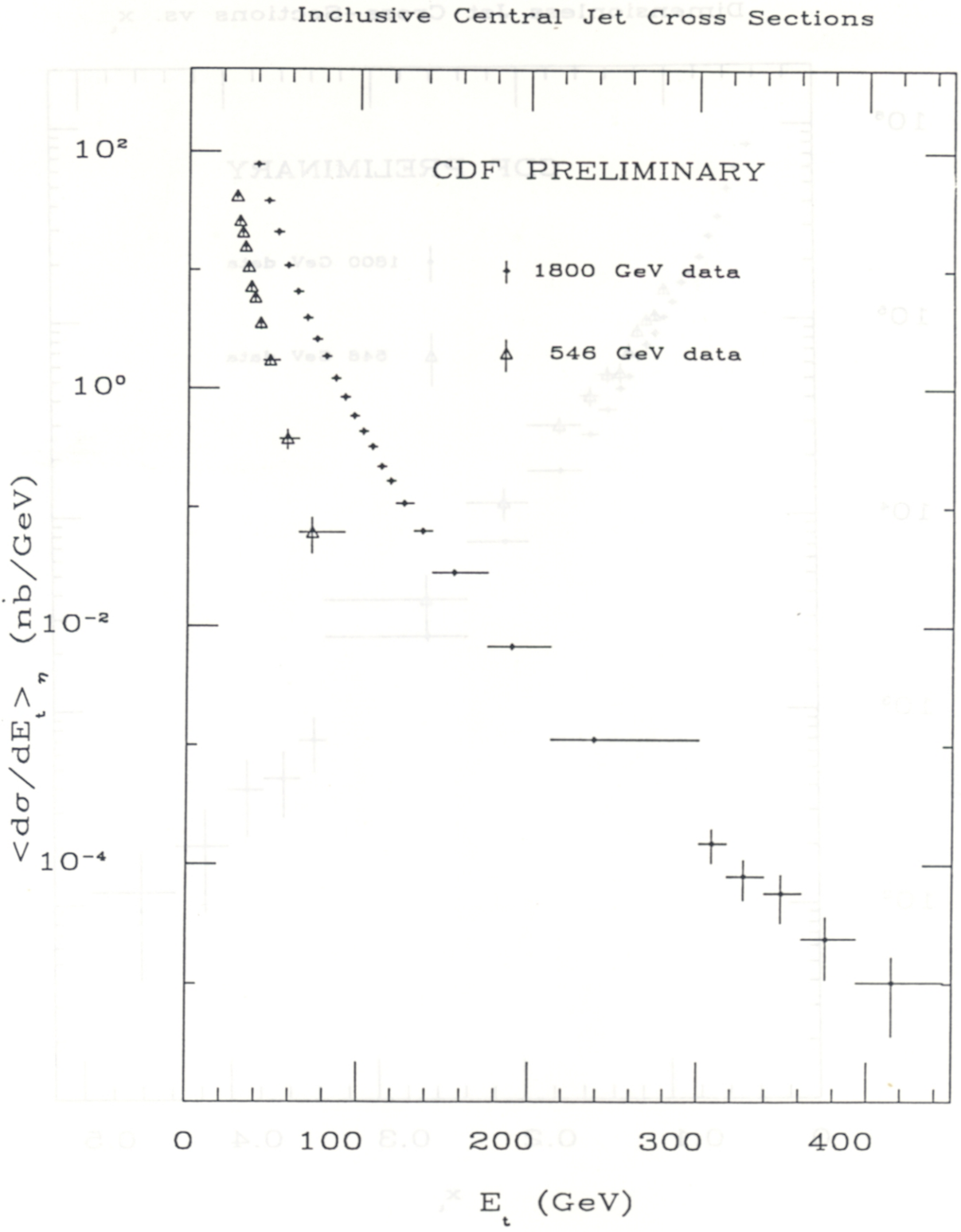
Inclusive Central Jet Cross Sections
CDF PRELIMINARY
1800 GeV data
546 GeV data
10^2
10^0
10^{-2}
10^{-4}
$<d\sigma/dE_t>_\eta$ (nb/GeV)
0
100
200
300
400
E_t (GeV)

FIGURE 26

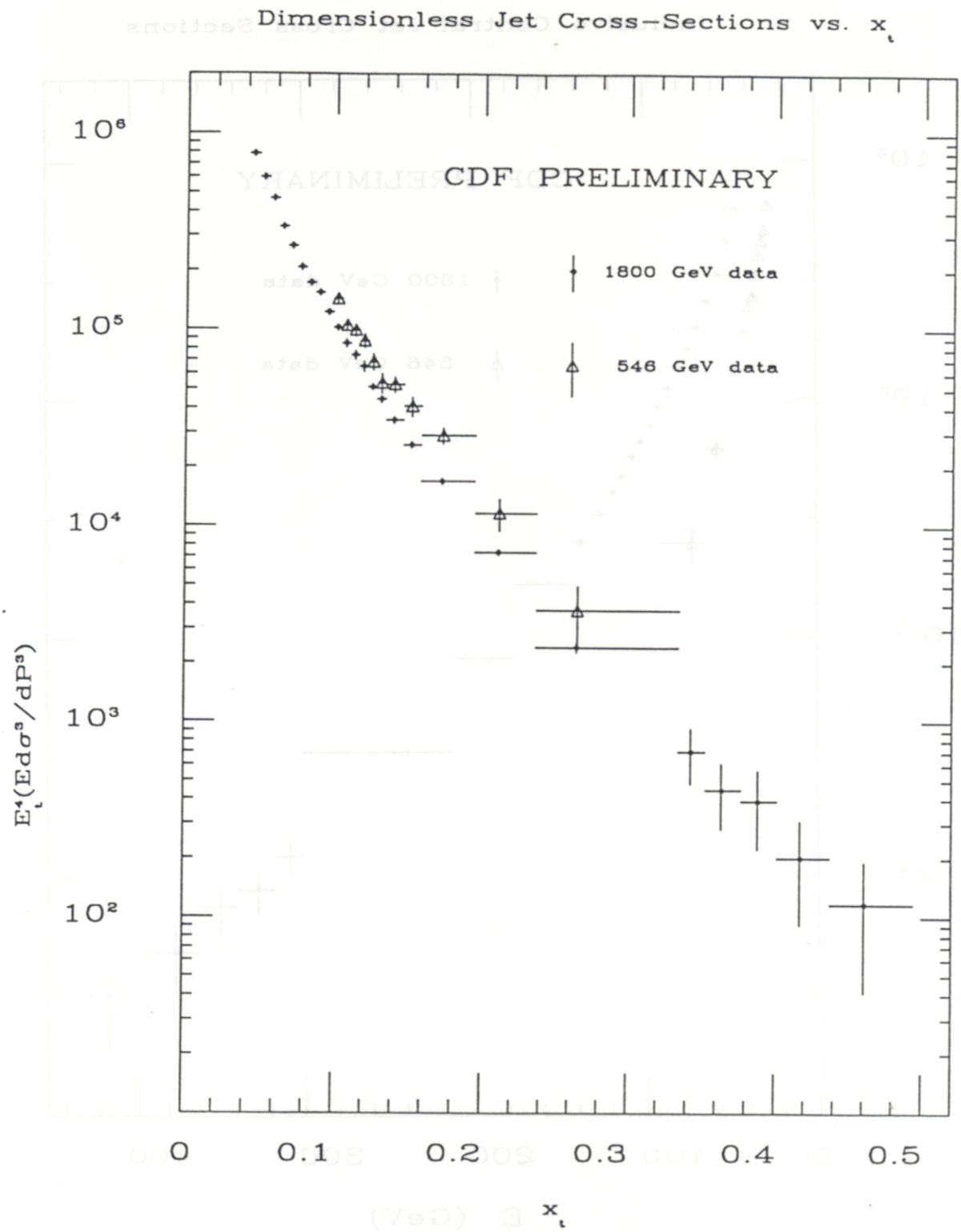
Dimensionless Jet Cross-Sections vs. x_t
CDF PRELIMINARY
1800 GeV data
546 GeV data
10^6
10^5
10^4
10^3
10^2
$E_t^4(Ed\sigma^3/dP^3)$
0
0.1
0.2
0.3
0.4
0.5
x_t

FIGURE 27

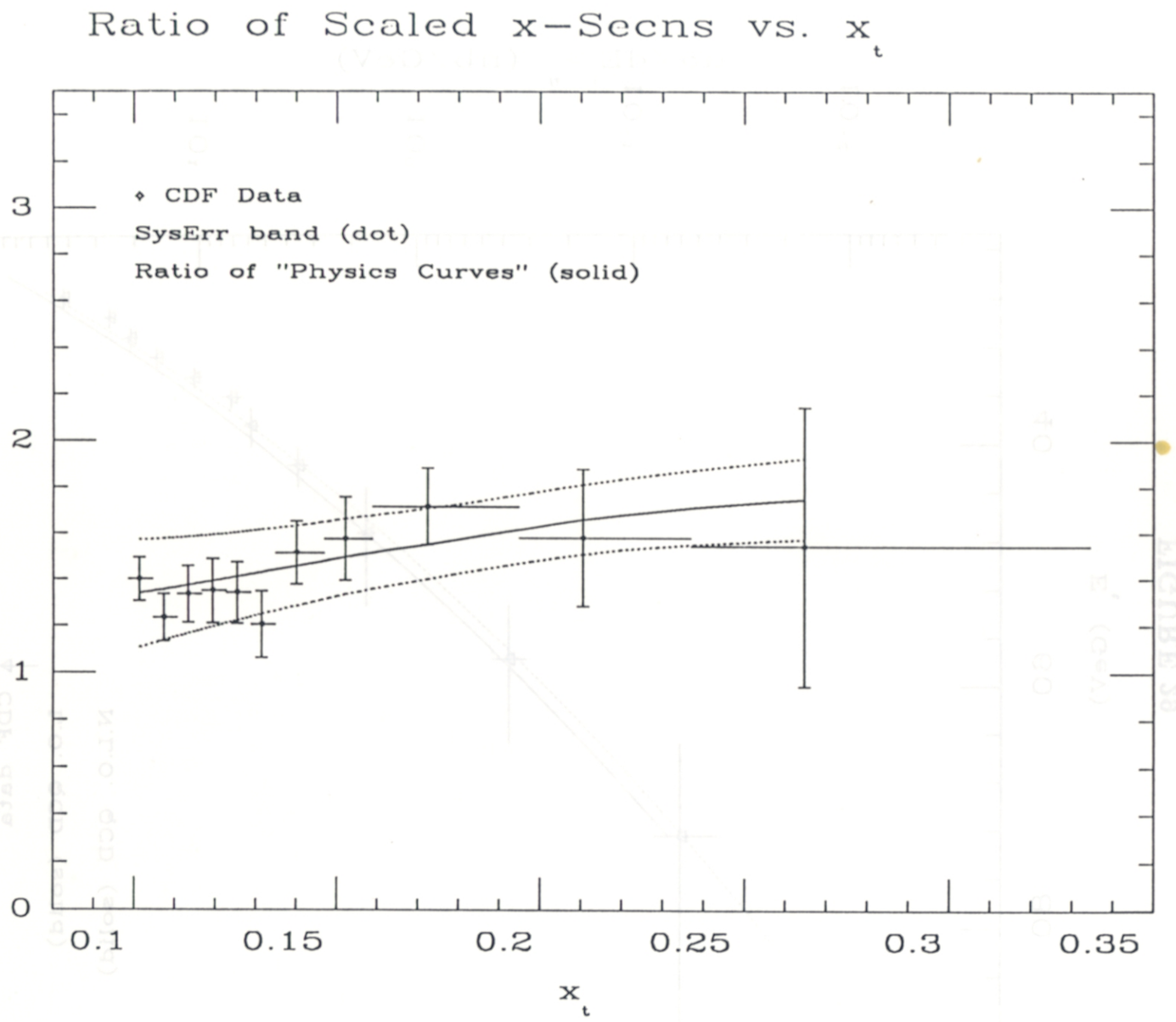
Ratio of Scaled x-Secns vs. x_t
◆ CDF Data
SysErr band (dot)
Ratio of "Physics Curves" (solid)
3
2
1
0
0.1
0.15
0.2
0.25
0.3
0.35
x_t

FIGURE 28

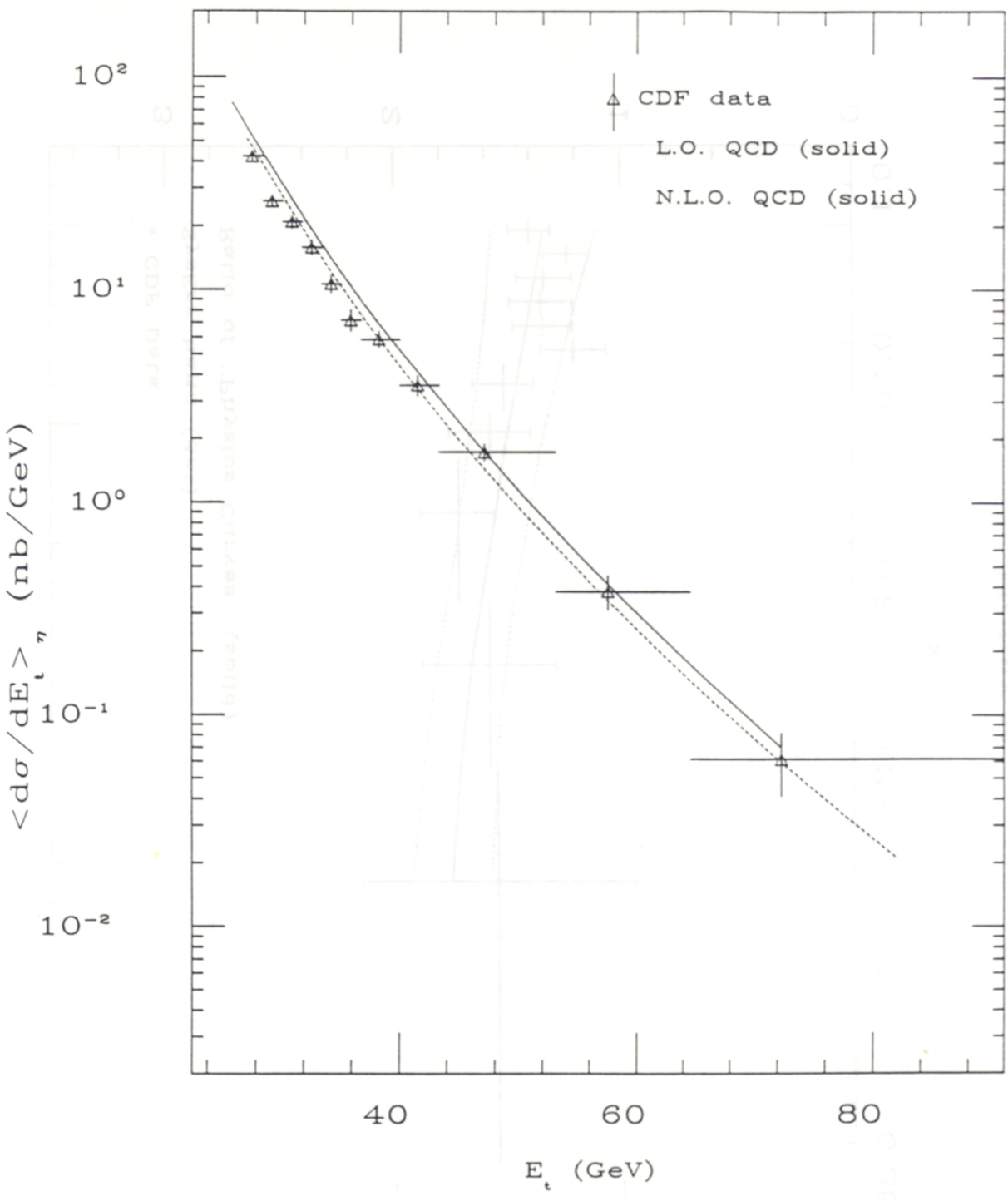
Inclusive Central Jet Cross Section, 546 Gev
CDF data
L.O. QCD (solid)
N.L.O. QCD (solid)
10^2
10^1
10^0
10^{-1}
10^{-2}
$<d\sigma/dE_t>_\eta$ (nb/GeV)
40
60
80
E_t (GeV)

FIGURE 29

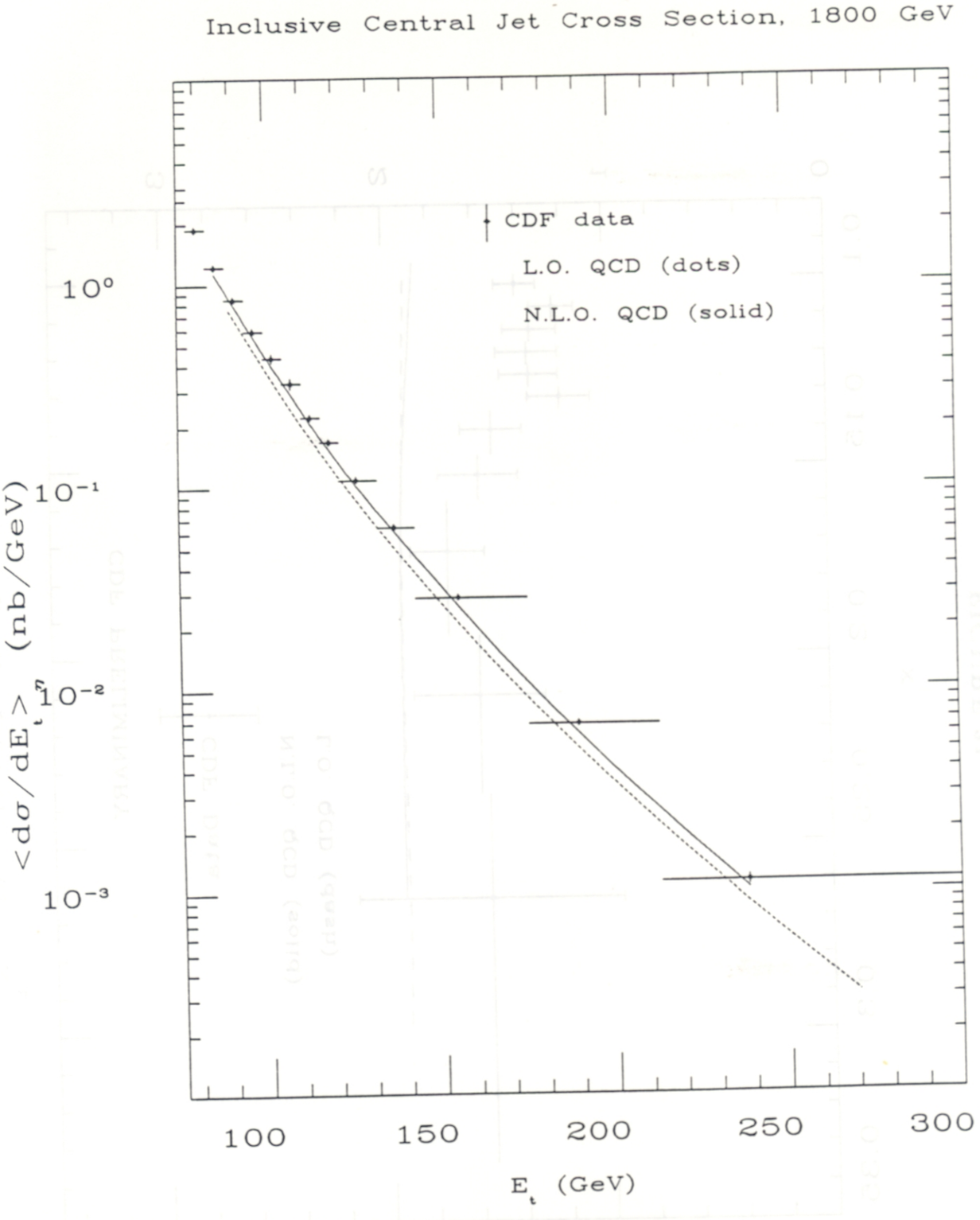
Inclusive Central Jet Cross Section, 1800 GeV
CDF data
L.O. QCD (dots)
N.L.O. QCD (solid)
10^{0}
10^{-1}
10^{-2}
10^{-3}
$<d\sigma/dE_t>^2$ (nb/GeV)
100
150
200
250
300
E_t (GeV)

FIGURE 30

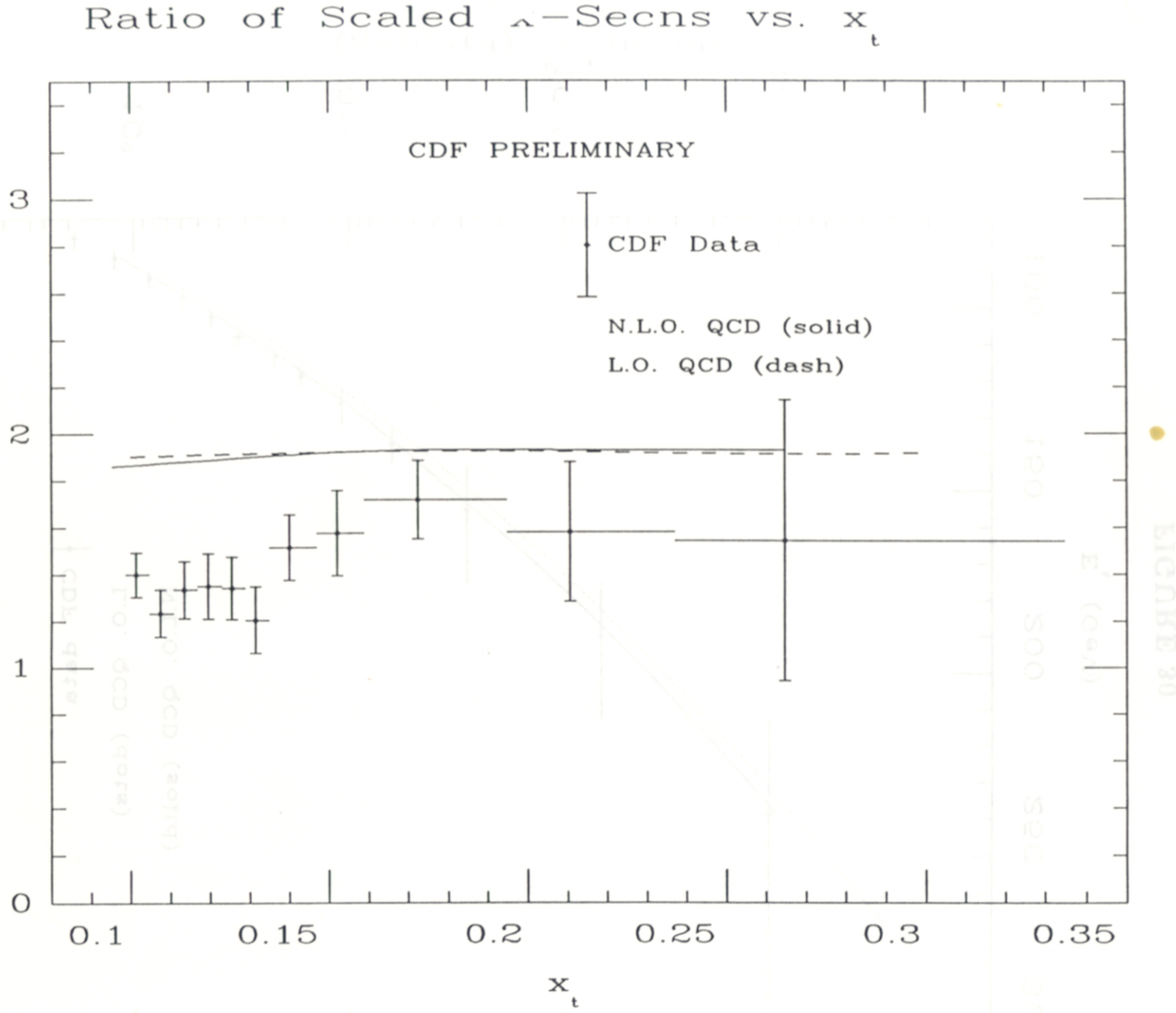
Ratio of Scaled Λ-Secns vs. x_t
CDF PRELIMINARY
CDF Data
N.L.O. QCD (solid)
L.O. QCD (dash)
0
1
2
3
0.1
0.15
0.2
0.25
0.3
0.35
x_t

FIGURE 31

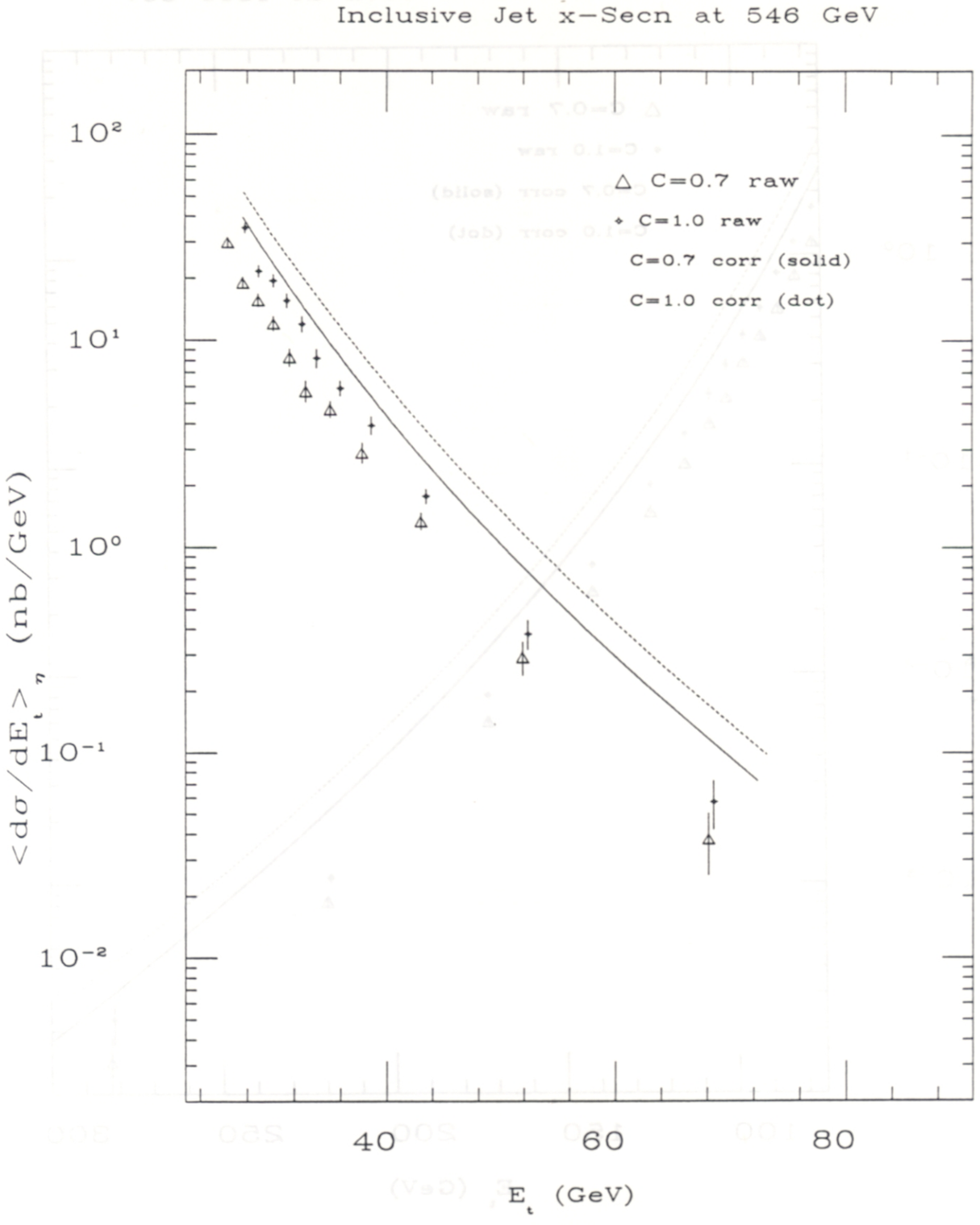
Inclusive Jet x−Secn at 546 GeV
△ C=0.7 raw
• C=1.0 raw
C=0.7 corr (solid)
C=1.0 corr (dot)
10²
10¹
10°
10⁻¹
10⁻²
<dσ/dE_t>_η (nb/GeV)
40
60
80
E_t (GeV)

FIGURE 32

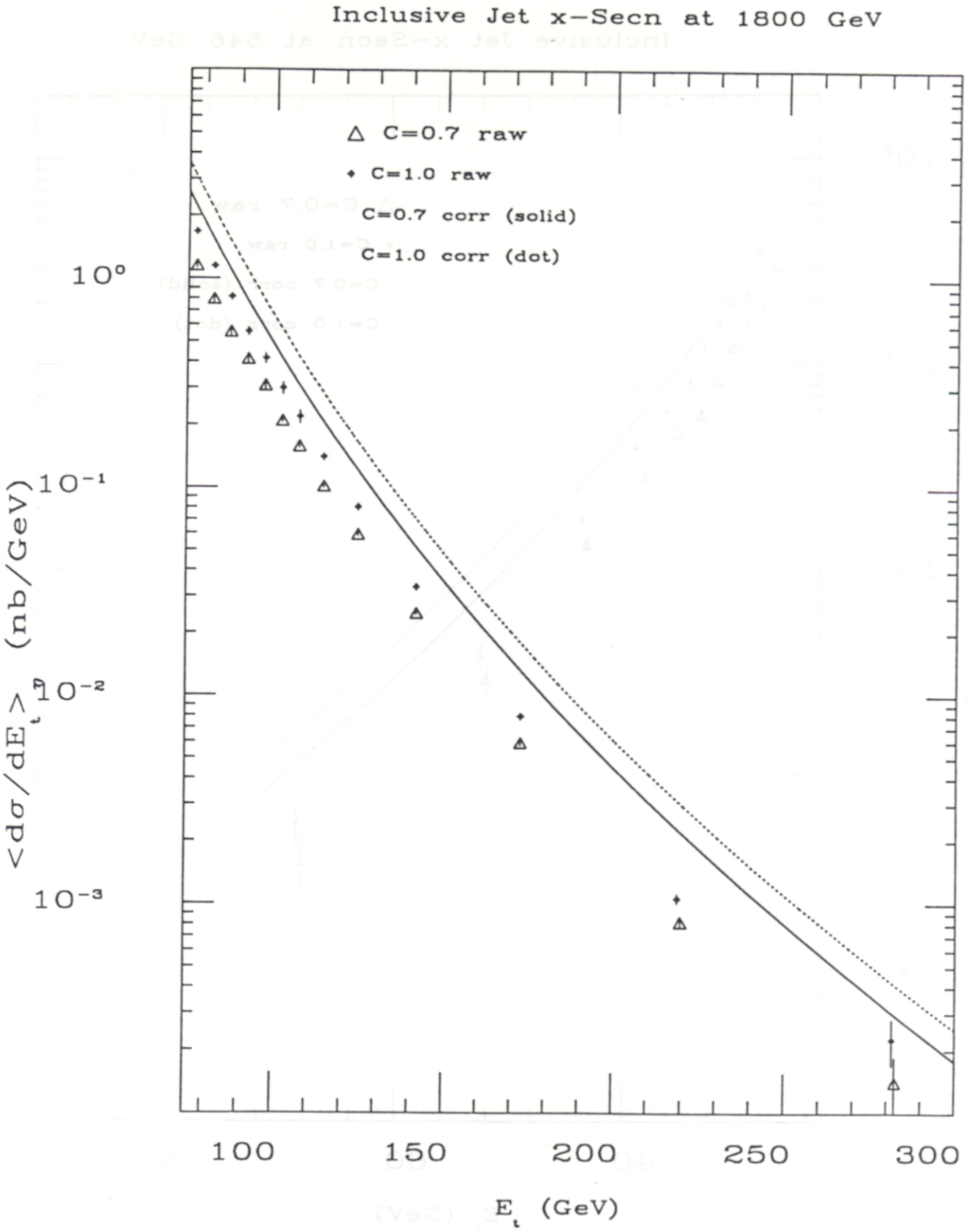
Inclusive Jet x−Secn at 1800 GeV
△ C=0.7 raw
• C=1.0 raw
C=0.7 corr (solid)
C=1.0 corr (dot)
10°
10⁻¹
10⁻²
10⁻³
<dσ/dE_t>_p (nb/GeV)
100
150
200
250
300
E_t (GeV)

FIGURE 33

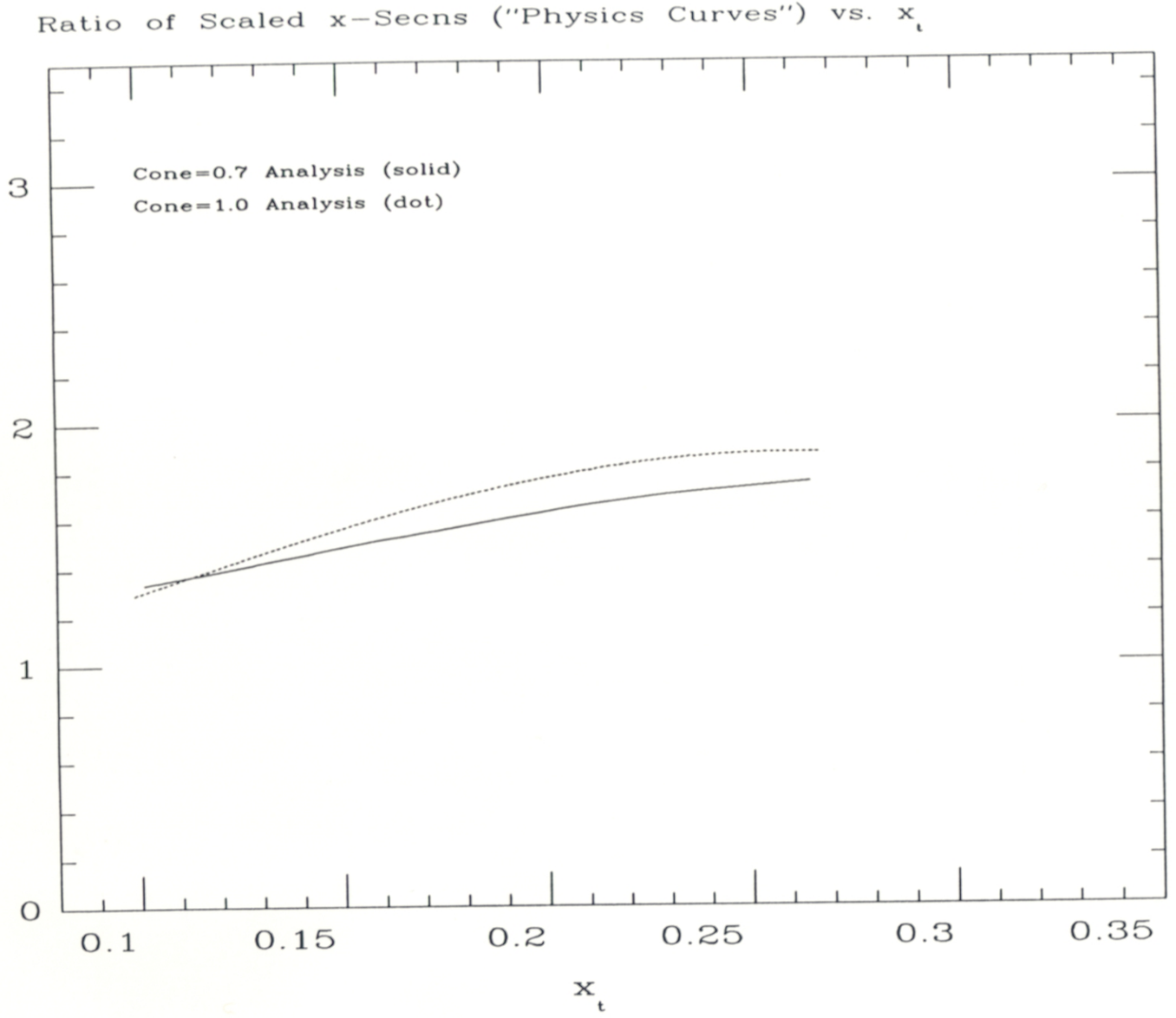
Ratio of Scaled x-Secns ("Physics Curves") vs. x_t
Cone=0.7 Analysis (solid)
Cone=1.0 Analysis (dot)
3
2
1
0
0.1
0.15
0.2
0.25
0.3
0.35
x_t

FIGURE 34